

Long-term variability of radio-bright BL Lacertae objects

Elina Nieppola, Talvikki Hovatta, Merja Tornikoski
Metsähovi Radio Observatory, TKK, Helsinki University of Technology
Metsähovintie 114, 02540 Kylmäla, Finland
elina.nieppola@tkk.fi

Esko Valtaoja
Tuorla Observatory
Väisäläntie 20, 21500 Piikkiö, Finland
Dept. of Physical Sciences, University of Turku, 20100 Turku, Finland
and

Margo F. Aller, Hugh D. Aller
Department of Astronomy, University of Michigan
Ann Arbor, MI 48109, USA

ABSTRACT

Radio-bright BL Lacertae objects (BLOs) are typically very variable and exhibit prominent flaring. We use a sample of 24 BLOs, regularly monitored at Metsähovi Radio Observatory, to get a clear idea of their flaring behavior in the radio domain and to find possible commonalities in their variability patterns. Our goal was to compare the results given by computational time scales and the observed variability parameters determined directly from the flux curves. Also, we wanted to find out if the BLO flares adhere to the generalized shock model, which gives a schematic explanation to the physical process giving rise to the variability. We use long-term monitoring data from 4.8, 8, 14.5, 22, 37, 90 and 230 GHz, obtained mainly from University of Michigan and Metsähovi Radio Observatories. The structure function, discrete correlation function and Lomb-Scargle periodogram time scales, calculated in a previous study, are analyzed in more detail. Also, we determine flare durations, rise and decay times, absolute and relative peak fluxes from the monitoring data. We find that radio-bright BLOs demonstrate a wide range of variability behavior, and few common denominators can be found. BLOs include sources with fast and strong variability, such as OJ 287, PKS 1749+096 and BL Lac, but also sources with more rolling fluctuations like PKS 0735+178. The most extreme flares can last for up to 13 years or have peak fluxes of approximately 12 Jy in the observer's frame. When the Doppler boosting effect is taken into account, the peak flux of a flare does not depend on the duration of the flare. A rough analysis of the time lags and peak flux evolution indicates that, typically, BLO flares in the mm – cm wavelengths are high-peaking, i.e., are in the adiabatic stage. Thus, the results concur with the generalized shock model, which assigns shocks travelling in the jet as the main cause for AGN variability. Comparing the computational time scales and the parameters obtained from the flux curve analysis (i.e., rise and decay times and intervals of the flares) reveals that they do have a significant correlation, albeit with large scatter.

Subject headings: galaxies: active – BL Lacertae objects: general – radio continuum: galaxies – methods: statistical – radiation mechanisms: non-thermal

1. Introduction

BL Lacertae objects (BLOs) are a relatively rare subclass of active galactic nuclei (AGN). Traditionally the defining properties of BLOs include a featureless optical spectrum, a flat radio spectrum and vigorous variability at all frequency bands (Stein et al. 1976; Kollgaard 1994; Jannuzi et al. 1994; Urry & Padovani 1995, and references therein). Most BLOs are thought to be highly beamed objects (Blandford & Königl 1979), which means that the

relativistic jets emanating from the core are pointing very closely at our direction. This is partly the cause of the featureless optical spectrum; the non-thermal continuum emission from the jet can swamp the thermal emission, including the emission lines, from the host galaxy. However, in the case of less beamed objects, the lineless spectrum must be created by other mechanisms.

The first BLO samples were discovered in either radio (Stickel et al. 1991, 1993) or X-ray surveys (Gioia et al. 1990; Stocke et al. 1991). Lately, surveys at differ-

ent wavelengths (Londish et al. 2002) and the cross-correlation of existing radio and other waveband catalogs (Perlman et al. 1998; Caccianiga et al. 1999; Landt et al. 2001; Giommi et al. 2005; Turriziani et al. 2007; Plotkin et al. 2008) have produced a large number of new members to the class. Typically the selection criteria are different from those of the pioneering surveys, which has widened the definition of a BL Lac object; hence, the variability characteristics of many of the newest BLOs are unknown due to lack of data.

In a recent paper (Nieppola et al. 2007), 37 GHz fractional variability indices from Metsähovi Radio Observatory data were calculated for 90 BLOs. All sources, for which even a crude estimation of variability could be calculated, exhibited an increase of 10 % of the minimum flux level at some point during the 3.5 year observation period. Almost half of them doubled their minimum flux density. However, this sample of 90 sources was only one fourth of the full Metsähovi BLO sample; the rest are too faint to allow any variability analysis.

The variability of BLOs, like all flaring AGN, is thought to be caused by shocks forming and travelling in the jet. The origin and early development of these shocks is not yet very well understood. Once propagating downstream in the jet, their evolution is easier to model with Compton, synchrotron and adiabatic losses (Marscher & Gear 1985; Hughes et al. 1989). Valtaoja et al. (1992) constructed a generalized view of the Marscher & Gear shock model, containing a general scenario of the AGN flare behavior, to be used in comparison with observations. The generalized model describes how the shape of the shock spectrum remains unchanged as its peak moves from higher to lower frequencies. The evolutionary track of the shock consists of growth ($S_m \propto \nu_m^a$), plateau ($S_m \approx \text{constant}$), and decay ($S_m \propto \nu_m^b$) stages, where S_m and ν_m are the turnover flux and frequency for the shock spectrum, and a and b are model-dependent parameters. The flares can ideally be divided into two groups: i) low-peaking flares, which will reach their maximum intensity at lower frequencies than the observing frequency, and ii) high-peaking flares, which have peaked at high frequencies relative to the observing frequency and are already decaying. The observing frequency, however, is not a constant quantity, but can be chosen freely. Thus the low- and high-peaking classes are not fixed either: the same flare can be low-peaking in one frequency band and high-peaking on another. Consequently, the classes are not separated, but rather opposite ends of a continuum of cases. Low- and high-peaking flares should be distinguishable from observations. For high-peaking flares the peak fluxes and time lags are strongly frequency-dependent, the highest observing frequency peaking first with the highest peak flux. For low-peaking flares the peaks are nearly simultaneous in all frequencies, and the peak flux of the flare is not significantly dependent on the frequency.

In this work we will study the long-term radio variability of BL Lacertae objects at several frequencies. We will focus on a sample of 24 BLOs. The current number of definite and probable BLOs is over 1000 (Véron-Cetty & Véron

2006). This means that our sample is not a representative cross-section for the whole population, but rather represents only the rare, radio luminous BLOs. The bases of our work are the extensive databases of Metsähovi and University of Michigan Radio Observatories at frequencies 4.8, 8, 14.5 GHz (UMRAO) and 22 and 37 GHz (Metsähovi).

We will study the variability of our BLO sample from two points of view: computational time scales obtained using statistical analysis methods and observed parameters of the flares, e.g. the duration, rise and decay times, and absolute and relative peak fluxes. The goal is to determine how well the computational time scales correspond to the behavior we observe in the source, as well as to gain a deeper understanding of what kind of variability can be expected from radio-luminous BLOs, when monitored for tens of years. We are also interested in how well the BLO flares adhere to the generalized shock model of Valtaoja et al. (1992), and whether the flares are mostly high- or low-peaking. A similar study is performed on a larger AGN sample, including radio-loud quasars, in an accompanying paper (Hovatta et al. 2008b).

In §2 we will present our sample and data. We briefly describe the methods we used in §3. In §§4 and 5 we discuss the time scales and the observed flux curves, respectively. In §6 we examine the correspondence between the time scales and observed flaring, and describe the behavior of the sample sources individually. We will finish with a discussion and conclusions in §§7 and 8, respectively. Throughout this paper, we assume $H_0 = 72 \text{ km s}^{-1} \text{ Mpc}^{-1}$, $\Omega_m = 0.27$, and $\Omega_\Lambda = 0.73$.

2. Sample and data

Our sample has been selected from the BLO sample monitored at the Metsähovi Radio Observatory for more than 20 years. The whole Metsähovi BLO sample comprises 398 sources, selected mainly from Véron-Cetty & Véron (2000). Most of the sources in the full sample are usually very faint or non-detectable (meaning $S/N \leq 4$) in the high radio frequencies (Nieppola et al. 2007). The sample in this study contains the very brightest sources with well-sampled flux curves. The selection criterion was ample data from a period of at least ten years in at least two radio frequencies. The sampling has to be sufficient to determine the peaks of possible flares with adequate accuracy. There are 24 available sources, 13 of which had one or several significant flares during the observing period. 2 of the BLOs are high-energy BLOs (HBLs), 4 intermediate BLOs (IBLs) and 18 low-energy BLOs (LBLs) (for the basis of this classification, see Nieppola et al. 2006). The source sample is listed in Table 1. Columns (1) and (2) give alternative names for the source, Cols. (3) and (4) give the right ascension and declination, respectively, Col (5) gives the redshift, Col (6) gives the Doppler boosting factor of the source taken from Hovatta et al. (2008c), and Col (7) gives the BLO class according to Nieppola et al. (2006). Column (8) indicates whether the source has been included in the flare analysis in this work, and Col (9) gives

the reference for the redshift.

We used seven different frequency bands in the analysis, covering the radio domain quite extensively. Low frequency data at 4.8, 8 and 14.5 GHz are from University of Michigan Radio Observatory. Details of the observing system and data reduction can be found in Aller et al. (1985). 22, 37 and 87 GHz data are from Metsähovi Radio Observatory (Salonen et al. 1987; Teräsrananta et al. 1992, 1998, 2004, 2005; Nieppola et al. 2007). The data reduction is described in Teräsrananta et al. (1998). The high frequency data at 90 and 230 GHz were obtained at the Swedish - ESO Submillimetre Telescope (SEST) in La Silla, Chile, from 1987 to 2003 (Tornikoski et al. 1996, and some unpublished data), and also collected from the literature (Steppe et al. 1988, 1992, 1993; Reuter et al. 1997). The 87 GHz archival data from Metsähovi were combined with the 90 GHz data to form the 90 GHz flux curve.

3. Methods

3.1. Time scales

The long term time scales of our sample have been calculated in Hovatta et al. (2007), where our sample represented the BLO class in comparison with other AGN subgroups. In this paper we report the individual time scales of the BLOs. The timescales have been calculated in three ways: using the structure function (SF), the discrete correlation function (DCF) and the Lomb-Scargle periodogram. DCF and periodogram may provide several time scales of different duration. In this paper we will concentrate only on the most significant ones. The theoretical aspects of the methods are discussed in Hovatta et al. (2007) and the references therein. In the interest of comparing them with the observed flux curves, we have kept the computational time scales in observer's frame throughout the paper and have not performed any redshift or Doppler corrections on them.

The three methods (T_{SF} , T_{DCF} , and T_P) respond to flux variations of different scales. SF is the most sensitive, picking up the short time scales and the structure of the flares, like the rise and decay times. DCF and L-S periodogram are meant to provide the time scale of longer variations, like the peak-to-peak intervals of major flares. The periodogram was originally developed to search for strict, sinusoidal periodicities. In this context it is used to give a characteristic time scale, and a result from the periodogram analysis does not mean that the source is strictly periodic. The distinctions of SF, DCF and periodogram are also thoroughly discussed in Hovatta et al. (2007).

3.2. Flare parameters

For comparison with the computational time scales, we determined some flare parameters directly from the observations. We use the word "flare" to describe a separate period of heightened activity. We have not separated the individual shocks contributing to the flux density rise, so in some cases one flare may include several components

but this is more pronounced in the low-frequency domain. The start and end times, and, thus, also the duration, of the flares are based on a careful visual estimation of each flux curve. Their error is dependent on the sampling frequency: with well-sampled flux curves the determination of the flares is more accurate. In 90 and 230 GHz the sampling was often too poor to allow the definition of the flares, which is why these frequencies are, in many cases, at least partly excluded from the analysis. A flare was included in the analysis if it was discernible at least at two frequencies, one of them being 22 or 37 GHz. The absolute peak flux and peak time are defined straightforwardly by the highest flux density measurement between the start and end times of the flare. The relative flux is defined as the difference between the flux minimum at the start of the flare and the absolute peak flux of the flare. The rise time is the interval between flare start and the time of the peak flux, while the decay time is the interval between the peak time and the end of the flare, defined as the flux minimum after the flare. No flare had a significant plateau stage. Unless clearly stated otherwise (see § 5.1), the flare parameters are also discussed in the observer's frame.

4. Time scales

The time scales are available for all frequencies that had a sufficiently well-sampled flux curve for their definition and are listed in Table 2. In many cases, only one or two methods could be utilized. There were two factors which complicated the determination of the time scales. Firstly, some sources are very faint and exhibit a relatively uneventful flux curve. In that case, the errors of the flux measurements are large compared to the flux densities. This leaves a considerable margin of error in the modest flux rises and falls, and adds to the uncertainties of the time scales. Secondly, some objects exhibit rapid variability and outbursts of different magnitudes, which results in many different time scales obtained in DCF and periodogram analyses. In the DCF analyses, we have chosen the first discernible peak, after the DCF has been on the negative side, as the representative time scale. In the case of the periodogram, the highest peak represents the most significant time scale. If such a peak occurred at a time scale that was longer than half of the total observing period, it was discarded to avoid spurious time scales. In some cases, the most significant DCF time scale is, for example, the second most significant according to the periodogram, in which case their values in Table 2 can be different.

There are some sources which have only a lower limit of T_{SF} listed in Table 2. In many cases, this lower limit time scale is long. We do not consider these as definite; rather, they are an indication that the determination of the time scale was difficult, often due to uneventful flux curves. ON 231 (see for Fig. 1 top panel for the flux curve at 22 GHz) is a good example of how one prominent flare can affect the determination of the time scales. It underwent a relatively strong outburst in the late 1970's - early 1980's, and the decay stage has been recorded in all frequency bands from 4.8 to 37 GHz. The more subtle flux variations are super-

posed on a steady decline of flux, which lasted from the very beginning of monitoring in the early 1980's to mid-1990's. While representing a valid variability time scale itself, this slow fluctuation hinders the definition of the shorter time scales. This affects mainly the SF, which is designed to distinguish the shortest time scales of variability, lengthening the time scale of these minor variations. As a result, most of the SF time scales calculated for ON 231 give only lower limits. Another example of a lower limit is the 22 GHz SF time scale of OQ 530 (see for Fig. 1 bottom panel for the flux curve at 22 GHz). Although the flux curves at 22 and 37 GHz are very similar, and time windows are comparable, the SF gives differing results. However, the structure of the SF is very complicated. At 22 GHz, hints of shorter time scales can be seen, but their plateaus in the SF are not clear enough to be picked as the representative time scale. Also, the 90 GHz DCF time scale of 1308+326 has exceptionally large errors, and the value should be treated with caution.

Studying the time scales of Table 2 more closely, we find that three objects, namely S5 0716+714, Mark 421 and PKS 1749+096, are among the five sources with the shortest time scales, independent of the method of calculation. Therefore, they can well be dubbed the BLOs with the fastest variability. Their shortest time scales vary from 70 days (T_{SF} for S5 0716+714 at 14.5 GHz) to 2.8 years (T_P for PKS 0754+100 at 37 GHz). It is noteworthy that Mark 421 has very low flux levels and the definition of the time scales suffers, as explained earlier. Other short time scale sources include OJ 287 (according to both SF and periodogram), PKS 0754+100, S4 0954+65, Mark 501, and 3C 371.0.

The objects 3C 446 and 1308+326 (according to both DCF and periodogram), OJ 425 (according to both SF and periodogram), as well as PKS 0735+178, ON 231, and 4C 14.60 seem to be good examples of sources with long time scales and slow variability. They have longest time scales ranging between 6.8 (T_{SF} for ON 231 at 4.8 GHz) and 15.2 years (T_P for 3C 446 at 8 GHz).

In general, the DCF and periodogram time scales have quite a good correspondence, and the SF time scales are clearly shorter (for more information on the correspondence of the time scales in general, see Hovatta et al. (2007)). For some sources, however, the differences between the time scales obtained with the three methods can be large. Usually this is because the most significant time scale is defined differently for these methods. In most cases when the periodogram and DCF time scales differ significantly, similar time scale to T_P has been seen also in the DCF but it has not been the most significant one. In some cases the different frequency bands have strikingly dissimilar values. This is typically due to the faintness of the source and the low amplitude variability, which can make the determination of a time scale a difficult task and overemphasize the influence of discrepant datapoints in the flux curve.

The mean values of T_{DCF} , T_{SF} and T_P for various AGN subgroups, including BLOs, are reported in Hovatta et al. (2007).

5. Observed radio outbursts

5.1. Flare morphology

There are 13 BLOs which exhibit significant flaring during our monitoring period. The flux curves of the flaring sources are available in Fig. 2 (Figures 2.2 – 2.13 are available in the online version of the journal), where each flare, identified at 22 or 37 GHz, is marked. It is evident that the flux curves are very diverse in morphology.

5.1.1. Sample means by source and frequency

The mean values of flare duration, rise time, decay time, absolute peak flux and relative peak flux, determined as described in §3.2 are listed in Table 3 for each of the 13 sources. The parameters have been calculated as an average for all frequency bands, and for 37 GHz separately for comparison. In one end we have objects like AO 0235+164, OJ 287, PKS 1749+096 and BL Lac itself with rapid and frequent fluctuations. In the other end of the range we find PKS 0735+178, 1308+326 and 3C 446 which have flares that last for several years, with only a couple of them covered by the span of our observations. In fact, there is much doubt about the nature of the latter objects. 1308+326 and 3C 446 were originally included in our BLO master list because several authors have classified them as borderline cases between BLOs and quasars (Gabuzda et al. 1993; Falomo et al. 1994; Laurent-Muehleisen et al. 1999; Aller et al. 1999). Later they have been listed as quasars in the Veron-Cetty & Veron Catalogs. While listed as BLO in Véron-Cetty & Véron (2006), PKS 0735+178 exhibits a similar type of radio flux curve.

The typical BLO flare has a measured peak flux well below 10 Jy, as seen in Table 3. The average relative peak fluxes are mostly below 5 Jy. The brightest flares in our sample are those of 3C 446, measured in both absolute and relative flux.

In Table 4 we present the minimum, maximum, mean and median values of flare duration and absolute and relative peak fluxes for each frequency used in our analysis. We calculated the relative peak fluxes in two different ways, first by subtraction ($S_{\max} - S_{\min}$) and secondly by division (S_{\max}/S_{\min}). The latter can be considered as a variability index for each flare. In the discussion of shock models (cf. Sect. 7) the first one is used. The duration and absolute peak flux of the flares are also tabulated in two different ways. We show the absolute duration in years and absolute peak flux in janskys for all the frequency bands and also the values of each individual flare normalized to the value at 22 GHz (in the calculation of the durations this was not possible for flare 2 of 1308+326 and flare 7 of BL Lac because their duration at 22 GHz could not be calculated).

There were 34 flares in total at 4.8 GHz, 38 at 8 GHz, 45 at 14.5, 22 and 37 GHz, 17 at 90 GHz and 8 at 230 GHz. In duration, the difference between the minimum and maximum values is vast. The majority of the flares are relatively short in duration for radio band events, and sources PKS 0735+178 and 1308+326 alone have flares extending over 6

years, as we already learned from Table 3. This can be seen in the median values in Table 4, which are between 2.3 and 2.7 years. The duration of the flares changes little with frequency which can be clearly seen in the relative durations. The absolute median values are slightly longer at 4.8 GHz and 8 GHz than in the higher frequencies, but only by 0.4 years at most. However, at 90 and 230 GHz the sparser sampling of the flux curves does not allow as accurate determination of the flare duration as the frequent sampling of the lower frequencies. In reality, the mean duration of the 90 and 230 GHz flares may be slightly shorter.

The absolute peak flux exhibits a stronger correlation with frequency. The flare peak fluxes range between 0.7 and 12.1 Jy. The median values rise with frequency up to 5.1 Jy at 37 GHz which is also seen when the normalized absolute peak fluxes are studied. In 90 and 230 GHz, the median peaks are more moderate, 4.4 and 3.2 Jy, respectively, corresponding to 90% and 67% of the flux at 22 GHz. Also in this case the sparse sampling of the highest frequencies has its effect: with more datapoints their median peak fluxes might be higher. The parameters of the relative flux behave roughly in the same manner. The relative fluxes of BLO flares range between 0.4 and 10.1 Jy. It is also seen that maximum fluxes are 1.4 to 18.5 times higher than minimum fluxes.

5.1.2. Flare intensity vs. duration

In Fig. 3 we have plotted the absolute peak flux, S_o , of each flare against the flare duration, t_o using all frequencies (top panel) and 37 GHz only (bottom panel). The distribution of the datapoints seems to be bimodal, with a dividing line running from the upper left corner to lower right. On a closer inspection we find that the datapoints in the upper right are those of the quasar-like objects PKS 0735+178, 1308+326 and 3C 446 (see §5.1.1). Their long and intense outbursts thus clearly differ from the typical BLO flares. Only one flare of 3C 446 is more BLO-like, as can be seen in Fig. 3.

We also find a distinct declining trend in both panels of Fig. 3. It is evident in both the typical BLOs and quasar-like objects, but less so in the latter, however, due to the one weak and short flare of 3C 446. The correlation for the “genuine” BLOs is significant also according to the Spearman rank correlation test. When all frequencies are considered, the Spearman correlation coefficient is $\rho = -0.238$ and the probability of no correlation $P = 0.001$. The strength of the correlation is slightly distorted by the fact that all the frequencies are included in the calculation, and thus every flare is counted for more than once. We also checked its significance at 4.8, 8, 14.5, 22 and 37 GHz separately. In this case, the significance of the correlation seems to vanish.

A natural explanation for the negative trend observed in Fig. 3 is the effect of Doppler boosting. In Eq. 1 the Doppler boosting factor is defined by the Lorentz factor of the jet flow Γ , speed of the jet β , and the viewing angle to

the line of sight of the observer θ .

$$D = \frac{1}{\Gamma(1 - \beta \cos \theta)} \quad (1)$$

As the boosting factor D increases, the internal time scales of the source get shorter and flux levels become higher. To better investigate the intrinsic properties of the sources, we plotted the Doppler-corrected peak luminosity, L_i , of each flare against the Doppler corrected duration, t_i , of the flare (Fig. 4). The corrections and luminosity calculation were performed with equations (see, e.g., Kembhavi & Narlikar (1999), but note the typing error in their Eq. (3.102))

$$t_i = \left(\frac{D_{var}}{1+z} \right) t_o \quad (2)$$

and

$$L_i = \left(\frac{1+z}{D_{var}} \right)^{3+\alpha} \frac{4\pi d_L}{1+z} S_o \quad (3)$$

where z stands for redshift and d_L for the luminosity distance. The subscripts i and o denote intrinsic and observational quantities, respectively. The Doppler factors D_{var} were taken from Hovatta et al. (2008c), where they have been determined from our extensive database of total flux density observations at 22 and 37 GHz in the same manner as in Lähteenmäki & Valtaoja (1999). Applying an exponential fit to individual shock components extracted from the flux curves gives the observed variability brightness temperature. Comparing it to the intrinsic brightness temperature gives the amount of boosting. In Eq. 3 we have assumed an evolving feature in the jet, in keeping with the shock scenario, and $\alpha = 0$ ($F \propto \nu^{-\alpha}$). For two sources in our flare analysis (S2 0109+22 and PKS 0422+004) no Doppler boosting factor was determined in Hovatta et al. (2008c) due to uncertain redshifts, and these are not included in Figs. 4 and 5.

Fig. 4 shows us that when the boosting effect is taken into account, the data set looks very different. Only 1308+326 has a strikingly long flare duration, followed closely by PKS 1413+135 at lower luminosities. There is no correlation between L_i and t_i among the “genuine” BLOs (black circles in Fig. 4) when all frequency bands are included ($\rho = 0.0939$ and $P = 0.1095$) or with 37 GHz datapoints only ($\rho = 0.1524$ and $P = 0.1986$). The difference between Figs. 3 and 4 attests again to the substantial influence the boosting effects have on our observations of AGN. The correlations are very similar using the relative flare luminosity.

5.1.3. Flare shapes

In 56% of all the flares the rise time Δt_R is shorter than the decay time Δt_D . The ratio of the decay time and rise time in logarithmic scale is plotted against the duration of the flare in Fig. 5, where the values have been corrected for relativistic boosting according to Eq. 2. In the top panel all flares in all frequencies are included, and in the bottom panel only the source-specific mean values are plotted. In

the top panel, the individual flares cover the available parameter space quite well. There are many flares in which the decay time is several times longer than the rise time and the mean ratio for all the flares is 1.61. The mean ratio for flares with decay time longer than the rise time is 2.32 while for sources with decay time shorter than the rise time the mean ratio is 0.67. In the case of the the source-specific mean values, however, the differences are more moderate, the average ratio being 1.59. This value corresponds reasonably well to the value 1.3 used by Valtaoja et al. (1999) in the exponential decomposition of radio flares. The difference between the values can be explained by different flare definition. In Valtaoja et al. (1999) individual shock components are used while in our approach an activity phase (which may include several shocks) is considered as a flare. On average, the decay times are longer than the rise times of the flares for all sources. However, as the top panel of Fig. 5 shows, one source can have flares of very diverse characteristics.

5.2. Time lags of the flare peaks

We made a qualitative analysis of the individual flares of our sample sources, tracking the order in which the flare moved from frequency band to the next and tracing the evolution of the peak flux from its maximum value. We used all available frequencies for each source. In flare 1 of 1308+326 and flare 3 of 3C 446, we took into account only the first component of the flare, although in some frequency bands other components may be stronger. Of the 45 flares included in our sample, 11 (24%) were consistent with the description of a high-peaking flare: the high frequencies peak first with the highest peak fluxes. There were nine (20%) more that were very nearly consistent, for example, with one frequency band peaking "too early". In four (9%) flares we possibly detected also the plateau stage in the high radio bands after which the flare turns into high-peaking. There was only one (2%) flare that was consistent with the low-peaking flare behavior (flare 9 of OJ 287, defined only at three frequency bands), and one that was nearly consistent (flare 4 of BL Lac). Four flares were entirely inconsistent with the shock model, having no sensible order in either the frequency or flux evolution. However, all these four flares occurred in sources with very fast and frequent variability (S5 0716+714, OJ 287, PKS 1749+096 and BL Lac), which means that the different flare components are particularly hard to separate. It is possible that this has affected our analysis. For a third of our flare sample, 15 flares in all, we could make no meaningful analysis of the time lags at all because of the sparse sampling of the flares.

We also calculated the time lags for 27 flares with sufficiently resolved structure. For some of them, time lags could be determined for only 2 or 3 frequency bands. The mean values of these tentative time delays range from roughly 10 days to 130 days in the observer's frame at 37 and 4.8 GHz, respectively. The mean and median values of errors in the peak times, in turn, are of the order of 28 and 10 days, respectively, for the whole sample. Thus, the precise time lags cannot be determined, but we chose rather

to examine the sequence in which the flare peak reaches each frequency. Each frequency band was assigned a rank number. The first frequency band which displayed the flare was ranked 1, the second was ranked 2 and so on.

Figure 6 shows a bubble plot of the peak time rank number plotted against frequency band. The size of each bubble is proportional to the number of cases having the same values of rank number and frequency. According to the general shock model of Valtaoja et al. (1992), in high-peaking flares, the higher frequencies peak first with the low frequencies following with increasing time delays. That is, if the flares followed the shock model precisely, we would see a negative correlation in Fig. 6, with the highest frequency peaking first (and having the lowest rank number) and other frequencies following in order. In Fig. 6 there certainly is a negative trend and the high frequencies have a lower rank numbers on average. A significant negative correlation is verified by the Spearman rank correlation test ($\rho=-0.567$ and $P < 0.0005$). In about half of the flares included in this analysis, the highest frequency band was the leading frequency band.

We plotted another bubble plot (Fig. 7) describing the dependency between the rank orders of relative peak fluxes ($S_{\max} - S_{\min}$) and the frequency. Of the relative fluxes, the highest was ranked first. According to the shock model, there should be again a negative correlation, which is indeed very strong ($\rho=-0.592$ and $P < 0.0005$ in the Spearman test). In the two highest frequency bands, 90 and 230 GHz, there are some stray datapoints in the high ranks. There is a strong possibility that the flares have not been detected in these frequencies in their full strength due to sparse sampling. The plot is very similar when the ratio of maximum and minimum fluxes is used as the relative flux.

One should, however, bear in mind that the unambiguous definition of the time lag of the flare peak from one frequency band to another is made difficult by the complex structure of some of the flares. When there are several flare components superposed on each other, it can be tricky to trace the evolution of just one of them. Also, the error range in the peak time can be substantial, depending on the sampling density.

6. The correspondence between time scales and flare parameters

6.1. Notes on individual sources

In the following, we present a brief description of the flaring sources and their behavior at all available frequency bands individually (flux curves of the sources are available in the electronic edition of the Journal). We also compare their flux curves to the time scales discussed in § 4.

S2 0109+22: Three distinct flares can be discerned at 4.8, 8, 14.5, 22 and 37 GHz; the higher frequencies are too sparsely sampled. The first two flares, peaking in 1993 and 1998, lasted for about 3 years, while the last one, in 2000, lasted for up to 6 years in the low frequencies. All three

were relatively weak; the 1998 flare had the highest peak flux of 3.13 Jy at 37 GHz. The third flare reached its peak in approximately one year, depending on the frequency, but took up to 5.6 years to decrease back to base level flux. The flares consist of multiple components, which makes it difficult to find the peak especially in the low frequency flux curves. In the first flare the 8 GHz flux peaks first, higher frequencies follow within a month. The 4.8 GHz flux peaks almost 6 months later. In the second one, 37 GHz leads, with the other frequencies peaking almost a year later, 4.8 GHz being the last again with a time lag of over a year.

The T_{SF} values for S2 0109+22 range from 0.86 (22 GHz) to 4.817 (8 GHz) yrs. In 22 GHz the flares are much stronger, and the SF is affected by the relatively well-sampled and fast rises and falls of the flares. In 8 GHz, the flux curve is less dramatic, and this can be seen as a longer T_{SF} . In 8, 14.5 and 22 GHz the DCF seems to pick up the interval between flares 1 and 3, giving time scales between 5.82 and 7.73 yrs. At 4.8 GHz, where the peaks of the flares are barely discernible, T_{DCF} = 1.85 yrs. At 37 GHz, the three flares are clearly above the base level flux, and more evenly separated. This affects also the DCF, which now gives a time scale of 2.94 yrs, a little more than half of the interval between flares 1 and 2, and almost exactly the interval between flares 2 and 3.

AO 0235+164: Here we have four distinguishable multifrequency flares in 1987, 1990, 1992 and 1998. The maximum peak fluxes are 4.44 Jy at 14.5 GHz, 4.20 Jy at 90 GHz, 6.88 Jy at 37 GHz and 5.56 Jy at 37 GHz, respectively. The flares have some substructure, but the peaks are still quite clearly defined. Although relatively intense, the flares last for 3 years or less in all frequencies. We were able to determine time lags for two flares. In both, the flare commences at 230 GHz. The other frequencies follow some tens of days later in a rather random order. The longest time delay, 104 days, is at 8 GHz in the 1987 flare, where 230 GHz was the leading frequency band.

The high level of activity in the total flux density flux curve for AO 0235+164 is reflected in its SF time scales, which are mostly below 1 yr. Only at 37 GHz, we find the most significant timescale to be T_{SF} = 2.71 yrs, but another timescale of T_{SF} = 0.87 yrs is also seen in the SF. The approximate intervals between flares 1–4 are 4, 2 and 6 years. We find roughly the same numbers listed in Table 2 as T_{DCF} and T_P . In most cases, the most significant time scale is around 5.5 years. In 4.8 GHz, the periodogram picks up an 11.5 -year time scale, which is twice the T_P of the other frequencies (see also § 4).

PKS 0422+004: The flux curves are quite poorly sampled, but two events can be discerned. One flare took place in 1994 with a peak flux of 1.37 Jy and another in late 2001 with a peak flux of 2.40 Jy. These low flux levels make every small variation stand out, hindering the clear definition of the flare. In the first the duration ranges from 2.3 to 6 years, depending on frequency band, while the second one lasted for about 2 years. In the second flare there

are no long time lags, all available frequencies peak within 37 days.

The T_{SF} obtained for PKS 0422+004 are mostly lower limits of approximately 10 years. For 14.5 and 37 GHz we got T_{SF} = 3.83 and T_{SF} = 2.71, respectively. The DCF did not produce any time scales at 22 and 37 GHz, and there were no time scales in the periodogram analyses of any of the frequency bands. In the lower frequencies, T_{DCF} = 6–7 years, which corresponds well to the interval of flares 1 and 2, which is about 7 years.

S5 0716+714: This source also has two multifrequency flares, in late 1998 and 2003. Both flares were monitored in radio frequencies up to 37 GHz, unfortunately high frequency data is missing. The first one peaked at 2.54 Jy, while the second one was considerably stronger at 6.28 Jy. Both peak fluxes occurred at 37 GHz. The latter flare was extensively monitored in a WEBT multifrequency campaign, including INTEGRAL (Ostorero et al. 2006). It was very fast, lasting approximately for 2.5 years. It is noteworthy that the absolute peak flux of the 2003 flare is strongly dependent on frequency. At 4.8 GHz it is only 1.9 Jy, and the flare barely stand out from the base level flux. From there on it steadily rises at each frequency to exceed 6 Jy at 37 GHz. The same effect can be seen in the 1998 flare, albeit to a lesser extent.

The SF time scales of S5 0716+714 seem to be either very fast ($T_{SF} \leq 1$ for 4.8, 14.5 and 37 GHz) or very long ($T_{SF} \geq 6$ for 8, 22 and 90 GHz). This discrepancy is most likely due to the sparser sampling of the prominent 2003 flare in 8, 22 and 90 GHz. Especially at 37 GHz it is very frequently sampled, and thus dominates the flux curve and time scales. The DCF and periodogram time scales are close to 5 years in 4.8 and 8 GHz, and roughly 2 years in the higher frequencies. The interval between flares 1 and 2 is of the order of 5 years. Thus, the two flares seem to define the time scales in the low frequencies, where they are very low in amplitude, but fail to do so from 14.5 GHz upward, where they are very strong. This is probably because of the increasing dominance of the 2003 flare, while at the same time the sampling in the beginning of the flux curve gets poorer in the higher frequencies.

PKS 0735+178: The flux curve is dominated by a single, double-peaked flare in all available frequencies. Frequent sampling and reasonably low short-term variability make its definition simple. The first component of the double peak was the stronger one in all frequencies except 4.8 GHz. The peak occurred in most frequencies in 1989, the peak flux was 5.30 Jy at 14.5 GHz. The duration of the flare was notably long, ranging from 10 to 12 years. The flux decline in particular was slow, lasting approximately 8 years.

The SF time scales, determined for frequencies up to 90 GHz, are diverse, ranging between 2.15 and 6.07 yrs. They are quite long, and the reason is evident in the flux curves: PKS 0735+178 has minimal short term flux variation. T_P

is available for only one frequency, 8 GHz, being 14.11 yrs. This clearly reflects the modest pace of the fluctuations of the flux curve. As the source only has one flare, it is impossible to comment on the compatibility of the flare intervals and time scales. The interval between the components of the double peak of flare 1 in of the order of 1.5 years at all frequencies, distinctly less than any time scale obtained in this analysis.

PKS 0754+100: This source exhibits two modest flares that have multifrequency data: one peaking in late 1996 and one in 2003. The peaks can be discerned quite effortlessly, although the flux levels are not very high. The first flare peaks at 2.94 Jy at 37 GHz and the latter at 2.57 Jy at 14.5 GHz. There was a more intense flare in the mid-1980's, peaking over 3 Jy at 8 and 14.5 GHz, but it was not monitored in Metsähovi and thus is not included in our analysis.

The T_{SF} , T_{DCF} and T_P values could be determined for all frequencies up to 37 GHz. They are not very consistent: T_{SF} is approximately 0.5 – 4.3 yrs, T_{DCF} and T_P both approximately 2.8 – 10.8 yrs. There is also a clear discrepancy between the low and high frequencies, the latter having much shorter time scales. Much of the inconsistencies are due to the 1980's flare which is included in the 4.8 – 14.5 GHz data, but missing from 22 and 37 GHz data. The flare was strong and broad, and thus it has lengthened the low frequency time scales. The interval between the two flares accounted for in this analysis is approximately 6.5 years at all frequencies, best reflected by the 22 GHz time scales. The longest time scale, $T_{DCF} = 10.88$ yrs is found at 14.5 GHz. In that frequency band, the peak of flare 1 is particularly well sampled and strong, probably strengthening the time scale corresponding to the interval between the 1980's flare and flare 1, which is roughly 12 years.

OJ 287: Being one of the most-studied sources in the Tuorla-Metsähovi observing project, OJ 287 has ample data. Its flux curves in all frequencies are characterized by vigorous variability superposed on a long-term fluctuation of the base level flux. The yearly mean values of flux density at 37 GHz range between almost 8 Jy and less than 2 Jy. The determination of single flares is very difficult due to the sheer number of them. We count as many as 9 multifrequency outbursts during the 25 years of our monitoring. They are quite brief in duration, typically lasting for less than two years, or, in many cases, less than a year. The highest peak flux, 9.63 Jy, occurred in 1983 at 22 GHz. The undertakings of OJ 287 are of special interest because of its claimed optical periodicity. This almost 12-year periodicity is thought to be possibly the result of a binary black hole interaction (Sillanpää et al. 1988; Lehto & Valtonen 1996; Valtonen et al. 2008).

The rapid and frequent outbursts result in very short SF time scales, between 0.2 and 0.5 years at all frequencies. The DCF time scales, however, determined for 8 and 37 – 230 GHz, are considerably longer. They range approx-

imately between 4 and 6.5 yrs. The DCF probably picks up also the base fluctuation, which can have a time scale as long as 20 years. The sole T_P value that could be calculated was 1.03 yrs at 90 GHz. It describes the source well: the calculation of the flare intervals gives mostly values below 2 years. The intervals between flares 1 and 2 as well as 6 and 7 are of the order of 5 years. There are, however, minor flares evident in the flux curves during those intervals as well, but they are not included in this analysis.

1308+326: This source had a flare that lasted for the entire 1990's. It peaked in 1992 at 4.37 Jy at 22 GHz. In the lower frequencies it was clearly double-peaked, and had several components also in 22 and 37 GHz. After a slow decline the flux levels soared again in 2003, reaching a peak flux of 3.5 Jy at 14.5 GHz. An optical period for the source has been reported (Fan et al. 2002), but no periodicity in the radio data has been detected to our knowledge.

The interval between the two flares of 1308+326 is 8 years at 8 GHz and roughly 11 years at 14.5 – 37 GHz. This is evident in the T_{DCF} -values, which are between 10.34 and 11.70 yrs. Pyatunina et al. (2007) derived an activity cycle of ≥ 14 yrs for this source, which also reflects its long time scales of variability. At 90 GHz, $T_{DCF} = 3.77$ yrs, but this value has exceptionally large errors and is based on a poorly sampled flux curve where the flares cannot be discerned properly. The periodogram gives mostly similar results as DCF. At 8 GHz $T_P = 14.59$ yrs, which is quite high compared to the T_{DCF} -values. The SF time scales range as $T_{SF} = 2.71 - 4.29$, telling that 1308+326 has little short term variability.

PKS 1413+135: The flux curves are very erratic, making it difficult to find well-defined outbursts. Two multifrequency events can be discerned. The first flare peaks at 4.55 Jy at 37 GHz in the end of the year 1990. The second peaks at the same frequency at 2.46 Jy 7 years later, in 1997. The peak of the latter flare in particular is ill-defined. There is a clear flux boost lasting for more than six years, during which there are several minor maxima in all frequencies. There is also a pronounced flare visible in the low frequency data in the early 1980's, but the high frequency data is missing.

Noteworthy is also the strong evolution of the flux curve with frequency. At 4.8 GHz the flux curve is all but flat, but gradually it gets more eventful towards higher frequencies. This is reflected by the time scales. Both T_{SF} and T_{DCF} are clearly longer in the low frequencies. T_{SF} is 2.71 yrs at 8 GHz and 1.52 at 37 GHz; T_{DCF} is 9.38 yrs at 4.8 and 8 GHz, declining slowly to 2.26 at 90 GHz. Curiously enough, T_P values seem to remain unaffected by the evolution of the flux curve with frequency, ranging between roughly 7 and 9 years. In addition, the 14.5 GHz time scales are affected by the 1980's flare which is not included in the high frequency data. The intervals of the flares are hard to determine because of the ambiguous definition of the peak of the second flare. At 8 GHz it is roughly 4 years, at 14.5 GHz 2 years and at 22 and 37 GHz roughly 7

years. Thus, it is approximately comparable to T_P , except at 14.5 GHz.

PKS 1749+096: This object exhibits violent variability. There are five multifrequency flares peaking in 1993, 1995, 1998, 2001 and 2002. The 1993 flare had the highest peak recorded in our data, 12.07 Jy at 90 GHz. Given the relative brevity of the flares and their intensity, PKS 1749+096 also exhibits some of the fastest grand-scale rises and declines of flux. For example, in the 1993 flare it reached the peak flux in approximately 80 days, rising over 9 Jy. While normally a flat spectrum source, as BLOs in general, this object has been reported to have an inverted spectrum during outbursts (Torniainen et al. 2005).

PKS 1749+096 is another example of a flux curve evolving with increasing frequency. The flares, barely discernible at 4.8 GHz, get more intense at higher frequencies. As in the case of PKS 1413+135, the evolution is reflected in the time scales, albeit less clearly. Mostly it can be seen in the T_{DCF} values. They decline from 4.45 yrs at 4.8 GHz to 1.30 yrs at 90 GHz. At 8 GHz, T_{DCF} is the longest, 6.78 yrs. The intervals between the flares 1 – 4 are roughly 2 – 3 years. The interval between flares 4 and 5 is approximately 1 year. Also, as with PKS 1413+135, the T_P seem to be less affected by the changing behavior of the flux curve with growing frequency. T_P has its highest value at 37 GHz, where $T_P = 9.81$. The SF time scales are quite short, below 2 years, except for 8 GHz ($T_{SF} = 2.15$) and 90 GHz ($T_{SF} = 3.04$). The beginning of the flux curve is particularly well-sampled and relatively stable at 8 GHz, which probably lengthens T_{SF} compared to the high frequencies, which have less data. On the whole, the time scales of 14.5 and 22 GHz seem to correspond best to the flares included in the analysis.

S5 2007+77: This BLO has one outburst, which was reasonably well-monitored also at the Metsähovi frequencies. It occurred in 1991-1992 and reached a peak flux of 3.69 Jy at 14.5 GHz. The low frequency flux curves reveal that the source was very variable also prior to that time, but since the early 1990's it has been in a quiescent state with only modest variability. Unfortunately, the flux curves are not very well-sampled and data from 8 GHz and the very highest frequencies, 90 and 230 GHz, are missing completely from the flare analysis.

The SF time scales are mostly the typical 0.5 – 2 yrs, only at 22 GHz it is as long as 3.83 yrs. The 22 GHz flux curve, however is under-sampled and the time scales are tentative at best. In 37 GHz, the T_{SF} did not show a plateau and no time scale could be determined. The rise and decay times of flare 1 are between 1 and 2 years, so T_{SF} at 4.8 and 14.5 GHz describe them accurately. T_{DCF} produced significant time scales only at 4.8, 8 and 37 GHz, and T_P only at 37 GHz. All values are approximately 2 – 3 years, roughly compatible with the 1980's flaring evident in the low frequency flux curves.

BL Lac: The archetype of all BL Lacertae objects certainly has a very variable flux curve. Unfortunately the major flare of early 1980's is not included in our analysis due to poor sampling in 22 and 37 GHz. Since then, however, we count nine multifrequency outbursts in 1987-1988, 1989, 1992, 1993, 1996, 1997-1998, 2000, 2002 and 2003. All are similar in shape in the higher frequencies, peaking at 3–6 Jy. At 4.8 and 8 GHz the 1987-1988 and 1996 flares (flares 1 and 5) are more prominent with fast rises, and outbursts following them seem to be partially superposed on their slow decline. With growing frequency, flares 1 and 5 seem to lose their dominance and blend into the other flares.

T_{SF} values are mostly below 1 year, except for 4.8 GHz ($T_{SF} = 3.83$) and 22 GHz ($T_{SF} = 2.41$). In the former case, flares 1 and 5 dominate the small scale variations, leading to a long SF time scale. Especially the decay time of flare 1 is long. In 22 GHz, the reason for a long SF time scale is less clear. In the case of T_{DCF} and T_P , long time scales clearly dominate. The typical values are $T_{DCF} = 7.5$ yrs and $T_P = 8.5$ yrs. This contrasts with the average flare interval of approximately 2 yrs. The reason for such long time scales is probably the strong flare on early 1980's, which is unequalled in flux density. This conclusion can also be drawn from the 8 GHz time scales. They are considerably shorter, $T_{DCF} = 2.81$ yrs and $T_P = 3.80$ yrs, while 8 GHz is also the only frequency that has data from the beginning of 1970's when BL Lac was very bright, flux levels being comparable to those of the 1980's flare.

3C 446: The flux curve is marked by three flares, two of them quite broad and strong. The first peaked approximately in 1990. In 230 GHz, however, the peak occurred as early as 1988, when the flux levels reached 11.71 Jy. The other two peaked in 1996 and 2000, at 6.30 Jy and 9.29 Jy, respectively, at 22 GHz. All outbursts have multiple components and frequency evolution is apparent.

3C 446 has relatively few short scale flux variations and rise and decay times of 3 to 4 yrs in flares 1 and 3. This can be seen in the SF time scales which are quite long, roughly $T_{SF} = 3$ yrs, except for 8 GHz, for which $T_{SF} = 1.5$ yrs. This could be due to either the randomly sampled early flux curve at 8 GHz, which is missing in other frequencies, or just minor variations. The DCF and periodogram time scales were significant only at the low frequencies, and T_{DCF} also at 90 GHz. All T_{DCF} and T_P are long, mostly roughly 10 years or above, reflecting the rather sedate behavior of the source. However, their behavior is not very consistent: at 14.5 GHz, $T_P = 5.71$ yrs which is considerably shorter than at 4.8 and 8 GHz, but $T_{DCF} = 11.16$ yrs which is clearly longer than at the lower frequencies. It is of the same order as the 12 -year activity cycle for 3C 446 obtained by Pyatunina et al. (2007). At 90 GHz, $T_{DCF} = 5.96$ yrs, which roughly corresponds to the 6 – 7 year interval between flares 1 and 2. The average interval between flares 2 and 3 is 3.5 – 5 years.

6.2. Correlations

In §6.1 we described in detail how, for each source, the time scales and the observed flux curve related to each other. To illustrate the correspondence between the time scales and the temporal parameters of the outbursts more quantitatively we plotted i) SF time scales of the source against both the rise times, Δt_R , and the decay times, Δt_D , of the flare, averaged for each source and frequency (Fig. 8), ii) DCF and periodogram time scales against the peak-to-peak intervals of consecutive flares, Δt_{PP} , averaged for each source and frequency (Fig. 9). In all the plots, the dashed line represents an ideal one-to-one correspondence. All parameters are observational and have not been corrected for redshift nor for Doppler boosting.

From Fig. 8 we see that the plot is very similar for both the rise and decay times. There is considerable scatter at low Δt_R and Δt_D on both sides of the one-to-one line, and at high values the SF time scales seem to be significantly shorter than Δt_D . The lower limits of T_{SF} were not included in the plot. According to the Spearman rank correlation test, there is a significant positive correlation between T_{SF} and both Δt_R and Δt_D . For rise times, $\rho=0.600$ and $P < 0.0005$, and for decay times $\rho=0.607$ and $P < 0.0005$.

The distribution of the T_{DCF} and T_P values plotted against Δt_{PP} (Fig. 9) are also scattered, but seems to roughly follow the one-to-one line. According to the Spearman test, the positive correlation is significant for both the DCF ($\rho=0.366$ and $P=0.005$) and periodogram ($\rho=0.420$ and $P=0.008$).

7. Discussion

Throughout this paper it is important to remember that this sample represents only a small fraction of the BLO population. Most BLOs are too faint in the radio frequencies, or even if their flux density is above the detection limit, they simply lack the long-term data needed for this kind of analysis. Also, the high-energy BLOs (HBLs) are sorely underrepresented: only two of them are included in the time scale analysis, and none at all in the flare analysis. It is also noteworthy that only 13 of the 24 sources included in the time scale analysis had significant, well-sampled flares to analyze during the observing period. Some of the remaining 11 sources simply do not have a very variable flux curve, which indicates that even some radio-bright BLOs are surprisingly steady emitters. For example, Mark 421, B2 1147+24, and Mark 501 have remarkably uneventful radio flux curves. This is also confirmed by other authors (e.g. Venturi et al. 2001; Błażejowski et al. 2005; Lichti et al. 2008).

While the shock-in-jet scenario gives the general guidelines of AGN variability and its causes, there are many additional factors, such as relativistic boosting, properties of the ambient medium, turbulence and bending of the jet (Marscher 1996), affecting the flux behavior we observe. These effects together with the shock mechanism generate the diverse flux curves observed also in our sample, rang-

ing from the rapid spikes of OJ 287 to the modest pace of 1308+326 and PKS 0735+178.

As stated in Sect. 5.2, there are two things that complicate the analysis of the time lags of the BLO flares: the very complex structure of most of the flares and the regrettably sparse sampling. The first affects especially the small flares, where it can be impossible to separate the components from each other and thus their evolution cannot be traced. The latter creates errors in both the peak time and peak flux of the flare. In many cases errors in the peak time in different frequency bands do not allow the unambiguous determination of the order in which the flare peak reaches each band.

In spite of these complications, we find that most of the BLO flares seem to be high-peaking in the radio frequencies, following the classification of Valtaoja et al. (1992). The possible detection of the flare peak plateau in S vs. $\log \nu$ -representation in some cases, and the relatively short time delays in the high radio frequencies lead us to believe that the BLO flares typically reach their maximum development stage in the mm-or sub-mm-wavelengths. There were 4 flares, which were inconsistent with the generalized shock model. This is probably due to errors in peak timing and the underlying complexity of the flare.

Our view of the high-peaking nature of BLO radio flares is supported by the general behavior of the multi-frequency flux curves. In many sources, most notably S2 0109+22, S5 0716+714, OJ 287 and PKS 1413+135 the increasing flare flux levels with increasing frequency are evident just by looking at the data. The base level fluxes do not rise as steeply, which suggests that the flux increase can be attributed to the flaring component, i.e., the shock. There are exceptions; for example, PKS 0735+178 and 1308+326 do not follow this rule to the same extent. As we saw in §5.1, their behavior stands out in other ways as well.

Helical / curved jets have also been suggested to be the cause of large variations in the flux curves of many BLOs. Villata & Raiteri (1999) developed a model to explain the spectral variations of Mark 501 with a helical jet produced by a binary black hole system. The model was able to describe the peculiar X-ray part of the SED very well but the low frequency optical to radio part remained fairly constant. They concluded that the low frequency variations could be due to inhomogeneities in the rotating jet or intrinsic brightness variations. Ostorero et al. (2004) applied the model to the SED and the radio and optical flux curves of AO 0235+164. The model was based on the 5.7 year quasi-periodicity suggested for the source by Raiteri et al. (2001). The periodic flares are explained by rotation of the helix. Observed signatures are similar to the shock model so that first the high frequency portion of the jet approaches the line of sight and Doppler boosting increases causing the flux density to rise. As the helix rotates, different frequency portions approach the line of sight and this way the time delays between the frequency bands can be explained. In their model, the non-periodic flares were explained with intrinsic brightness variations (e.g. shocks). As the model was based on the observed

periodicity of 5.7 years, it should be modified now that the period did not repeat after the year 2000 Raiteri et al. (2006). It should be noted that the sources in our sample are not strictly periodic in the radio regime and usually the observed quasi-periodicities last only a short time in the flux curve (Hovatta et al. 2008a).

The model by Villata & Raiteri (1999) has also been used to explain the variations in BLOs S4 0954+65 (Raiteri et al. 1999), ON 231 (Sobrito et al. 2001) and S5 0716+714 (Ostorero et al. 2001, using data prior to the extreme flare in 2003). In addition, VLBI polarization observations have revealed helical magnetic fields in many BLOs (e.g. Gabuzda et al. 2004; Mahmud & Gabuzda, 2008). Some of those are also in our sample, but they are mostly sources for which we have not performed detailed flare analysis because they do not have distinct flares in the radio frequencies. It is indeed possible that in these sources the variations are caused by changes in the Doppler beaming due to curved jets rather than intrinsic phenomena like shocks. However, testing this scenario would require detailed studies of simultaneous SEDs, which is beyond the scope of this paper.

We showed in §6 that the computational time scales correlate fairly well with the observed temporal parameters. To our knowledge, such a straightforward, but revealing comparison has not been done before. The statistically significant correlation in Figs. 8 and 9 confirms that the SF, DCF and L-S periodogram time scales are indeed directly linked to the source behavior we observe. Unfortunately, the scatter is substantial. For example, in our data a source with a DCF time scale close to 8 years, can have real peak-to-peak flare interval of 2 to 10 years. The average absolute deviation of the computed time scale from the one-to-one correspondence is 0.98 and 1.24 years for T_{SF} against Δt_R and Δt_D , respectively, and 2.24 and 3.23 years for T_{DCF} and T_P against Δt_{PP} , respectively. In representing the peak-to-peak intervals of the flares, T_{DCF} and T_P are near equivalent. However, at least in the cases of PKS 1413+135 and PKS 1749+096, the periodogram results are less affected by the frequency evolution of the flux curve between the frequency bands.

Variability of BLOs in the lower radio frequencies of 4.8, 8 and 14.5 GHz was also studied by Aller et al. (1999). They studied the variability behavior of a complete flux-limited sample of 41 BLOs using e.g. the SF. Only two of the BLOs in our sample (OJ 425 and 4C 56.27) are not included in the sample of Aller et al. (1999). They used UMRAO data from 1980 to 1996, while we have used the same database updated until April 2005. We have compared our results to see if the source behavior has changed during the past ten years. On average, the time scales have remained quite similar, the average longest time scale from SF in Aller et al. (1999) is 2.9 years compared to our average SF time scale for BLOs which is 3.7 years (median is 2.7 years) (Hovatta et al. 2007). When individual sources are studied, there are some differences and we believe it is mainly due to the longer dataset used in our analysis. Similar results were obtained in Hovatta et al. (2007) when the

SF time scales for the whole AGN sample at 22 and 37 GHz were compared to analyses made ten years earlier.

In many of the BLOs in our sample short intraday variations are seen in optical and radio frequencies (e.g. Wagner & Witzel 1995). However, the sampling density of our monitoring programs is not frequent enough to detect such rapid variations, unless a special campaign is arranged. The only example for which intraday variations have been observed at 37 GHz using Metsähovi data is S5 0716+714 (Ostorero et al. 2006). During the extreme flare in 2003 a rapid flux rise of 42% was observed in a time period of 0.12 days. During the observing campaign the source was observed multiple times in a day, while usually our sampling density is of the order of a week. Ostorero et al. (2006) also concluded that the rapid variations are intrinsic to the source and not caused by interstellar scintillation (ISS), which is a more pronounced phenomenon at low radio frequencies. Rickett et al. (2006) have studied ISS of 146 extragalactic radio sources at 2 and 8 GHz, and their sample includes 13 sources which are also in our sample. For these sources the typical ISS timescales range from 2.9 to 10.4 days at 2 GHz and from 4.4 to 18.6 days at 8 GHz. Also, the ISS contribution is much weaker at 8 GHz than at 2 GHz. The timescales are so short that the variations caused by ISS would mostly not be seen in our observations. They also conclude that for some of the well-studied BLOs in our sample (e.g. AO 0235+164, PKS 1749+096 and BL Lac) it is clear that intrinsic variations dominate. Therefore we do not think that our results are affected by ISS.

8. Conclusions

We have studied the long-term radio variability and the flare morphology of radio-bright BL Lacertae objects. The main conclusions are as follows:

1. Radio-bright BLOs exhibit a range of flaring behavior, with few common features. Especially the quasar-like objects PKS 0735+178, 1308+326 and 3C 446 have distinctively long outbursts with modest short-term variability, contrasting with the more erratic behavior of other sample sources. The long flare of 1308+326 clearly stands out from the rest of the sample even after correcting for the relativistic boosting effects. Our findings confirm the quasar-like nature of 1308+326 and 3C446 and indicate that PKS 0735+178 also has radio behavior different from typical BLOs.
2. The median duration of a flare in a radio-bright BLO is of the order of 2.5 years, and the peak flux density typically reaches about 5 Jy at 37 GHz. On average, the decay time of the flare is 1.6 times longer than the rise time. When the Doppler boosting effect is taken into account, the peak flux of the flare does not depend on the duration of the flare, indicating that the energy release in a flare does not depend on its duration.

3. The 45 BLO flares in our analysis confirm the generalized shock model of Valtaoja et al. (1992) with no clear, undisputed exceptions. However, very frequent sampling on several radio frequencies is needed for the accurate, observational determination of the flare components and time lags. Based on the evolution of the relative peak flux and the time lags from one frequency band to the next, we find that the BLO flares are mostly high-peaking. Probably they reach their maximum development in the mm- to sub-mm-wavelengths.
4. The computational time scales, T_{SF} , T_{DCF} and T_P , have a statistically significant correlation with the temporal flare parameters obtained directly from the flux curves. However, scatter is considerable, and the average deviation from one-to-one correspondence is of the order of 1 - 3 years, depending on the parameter and time scale in question.

We gratefully acknowledge the funding from the Academy of Finland (project numbers 205793, 210338 and 212656). UMRAO is supported in part by a series of grants from the NSF, most recently AST 0607523, and by funds from the University of Michigan Department of Astronomy.

REFERENCES

- Aller, H. D., Aller, M. F., Latimer, G. E., & Hodge, P. E. 1985, *ApJS*, 59, 513
- Aller, M. F., Aller, H. D., Hughes, P. A., & Latimer, G. E. 1999, *ApJ*, 512, 601
- Blandford, R. D. & Königl, A. 1979, *ApJ*, 232, 34
- Błażejowski, M., Blaylock, G., Bond, I. H. et al. 2005, *ApJ*, 630, 130
- Britzen, S., Vermeulen, R. C., Campbell, R. M., et al. 2008, *A&A*, 484, 119
- Caccianiga, A., Maccacaro, T., Wolter, A., della Ceca, R., & Gioia, I. M. 1999, *ApJ*, 513, 51
- Carangelo, N., Falomo, R., Kotilainen, J., Treves, A., & Ulrich, M.-H. 2003, *A&A*, 412, 651
- Cohen, R. D., Smith, H. E., Junkkarinen, V. T. & Burbidge, E. M. 1987, *ApJ*, 318, 577
- de Grijp, M. H. K., Keel, W. C., Miley, G. K., Goudfrooij, P., & Lub, J. 1992, *A&AS*, 96, 389
- Falomo, R., Scarpa, R. & Bersanelli, M. 1994, *ApJS*, 93, 125
- Fan, J., Lin, R., Xie, G., et al. 2002, *A&A*, 381, 1
- Gabuzda, D. C., Kollgaard, R. I., Roberts, D. H., & Wardle, J. F. C. 1993, *ApJ*, 410, 39
- Gabuzda, D. C., Murray, É., & Cronin, P. 2004, *MNRAS*, 351, L89
- Gioia, I., Maccacaro, T., Schild, R., et al. 1990, *ApJS*, 72, 567
- Giommi, P., Piranomonte, S., Perri, M., & Padovani, P. 2005, *A&A*, 434, 385
- Hewitt, A. & Burbidge, G. 1987, *ApJS*, 63, 1
- Hewitt, A. & Burbidge, G. 1989, *ApJS*, 69, 1
- Hovatta, T., Lehto, H. J., & Tornikoski, M. 2008a, *A&A*, 488, 897
- Hovatta, T., Nieppola, E., Tornikoski, M., et al. 2008b, *A&A*, 485, 51
- Hovatta, T., Tornikoski, M., Lainela, M., et al. 2007, *A&A*, 469, 899
- Hovatta, T., Valtaoja, E., Tornikoski, M., & Lähteenmäki, A., 2008c, *A&A* in press, arXiv:0811.4278
- Hughes, P. A., Aller, H. D., & Aller, M. F. 1989, *ApJ*, 341, 54
- Jannuzi, B. T., Smith, P. S., & Elston, R. 1994, *ApJ*, 428, 130
- Kembhavi, A. K. & Narlikar, J. V. 1999, *Quasars and active galactic nuclei : an introduction*, Cambridge University Press. ISBN 0521474779.
- Kollgaard, R. I. 1994, *Vistas in Astronomy*, 38, 29
- Lähteenmäki, A. & Valtaoja, E. 1999, *ApJ*, 521, 493
- Landt, H., Padovani, P., Perlman, E. S., et al. 2001, *MNRAS*, 323, 757
- Laurent-Muehleisen, S. A., Kollgaard, R. I., Feihgelson, E. D., Brinkmann, W. & Siebert, J. 1999, *ApJ*, 525, 127
- Lawrence, C. R., Pearson, T. J., Readhead, A. C. S. & Unwin, S. C. 1986, *AJ*, 91, 494
- Lehto, H. J. & Valtonen, M. J. 1996, *ApJ*, 460, 207
- Lichti, G. G., Bottacini, E., Ajello, M. et al. 2008, *A&A*, 486, 721
- Londish, D., Croom, S., Boyle, B., et al. 2002, *MNRAS*, 334, 941
- Mahmud, M. & Gabuzda, D. C., *ASPC*, 386, 494
- Marscher, A. P. 1996, *ASPC*, 110, 248
- Marscher, A. P. & Gear, W. K. 1985, *ApJ*, 298, 114
- Nieppola, E., Tornikoski, M., Lähteenmäki, A., et al. 2007, *AJ*, 133, 1947
- Nieppola, E., Tornikoski, M., & Valtaoja, E. 2006, *A&A*, 445, 441
- Nilsson, K., Pursimo, T., Sillanpää, A., Takalo, L. O. & Lindfors, E. 2008, *A&A*, 487, L29
- Ostorero, L., Raiteri, C. M., Villata, M., et al. 2001, *Mem. S.A.It.*, 72, 147
- Ostorero, L., Villata, M., & Raiteri, C. M. 2001, *A&A*, 419, 913
- Ostorero, L., Wagner, S., Gracia, J., et al. 2006, *A&A*, 451, 797
- Perlman, E. S., Padovani, P., Giommi, P., et al. 1998, *AJ*, 115, 1253
- Plotkin, R. M., Anderson, S. F., Hall, P. B., et al. 2008, *AJ*, 135, 2453
- Pyatunina, T. B., Kudryavtseva, N. A., Gabuzda, D. C., et al. 2007, *MNRAS*, 381, 797
- Raiteri, C. M., Villata, M. Tosti, G., et al. 1999, *A&A*, 352, 19
- Raiteri, C., Villata, M., Aller, H. D., et al. 2001, *A&A*, 377, 396

- Raiteri, C. M., Villata, M., Kadler, M., et al. 2006, *A&A*, 459, 731
- Reuter, H.-P., Kramer, C., Sievers, A., et al. 1997, *A&AS*, 122, 271
- Ricket, B. J., Lazio, T. J. W., & Ghigo, F. D. 2006, *ApJS*, 165, 439
- Salonen, E., Teräsraanta, H., Urpo, S., et al. 1987, *A&AS*, 70, 409
- Sillanpää, A., Haarala, S., Valtonen, M. J., Sundelius, B., & Byrd, G. G. 1988, *ApJ*, 325, 628
- Smith, A. G. & Nair, A. D. 1995, *PASP*, 107, 863
- Sobrito, G., Raiteri, C. M., Villata M. et al. 2001, *Mem. S.A.It.*, 72, 149
- Sowards-Emmerd, D., Romani, R. W., Michelson, P. F., Healey, S. E. & Nolan, P. L. 2005, *ApJ*, 626, 95
- Stein, W. A., O'Dell, S. L., & Strittmatter, P. A. 1976, *ARA&A*, 14, 173
- Steppe, H., Liechti, S., Mauersberger, R., et al. 1992, *A&AS*, 96, 441
- Steppe, H., Paubert, G., Sievers, A., et al. 1993, *A&AS*, 102, 611
- Steppe, H., Salter, C. J., Chini, R., et al. 1988, *A&AS*, 75, 317
- Stickel, M., Fried, J. W., & Kuehr, H. 1988, *A&A*, 191, L16
- Stickel, M., Fried, J. W., & Kuehr, H. 1989, *A&AS*, 80, 103
- Stickel, M., Fried, J., & Kühn, H. 1993, *A&AS*, 98, 393
- Stickel, M., Fried, J. W., Kuehr, H., Padovani, P. & Urry, C. M. 1991, *ApJ*, 374, 431
- Stoeke, J. T., Morris, S. L., Gioia, I. M., et al. 1991, *ApJS*, 76, 813
- Teräsraanta, H., Achren, J., Hanski, M., et al. 2004, *A&A*, 427, 769
- Teräsraanta, H., Tornikoski, M., Mujunen, A., et al. 1998, *A&AS*, 132, 305
- Teräsraanta, H., Tornikoski, M., Valtaoja, E., et al. 1992, *A&AS*, 94, 121
- Teräsraanta, H., Wiren, S., Koivisto, P., Saarinen, V., & Hovatta, T. 2005, *A&A*, 440, 409
- Torniainen, I., Tornikoski, M., Teräsraanta, H., F., A. M., & H., A. 2005, *A&A*, 435, 839
- Tornikoski, M., Valtaoja, E., Teräsraanta, H., et al. 1996, *A&AS*, 116, 157
- Turriziani, S., Cavazzuti, E., & Giommi, P. 2007, *A&A*, 472, 699
- Tytler, D. & Fan, X.-M. 1992, *ApJS*, 79, 1
- Ulrich, M.-H., Kinman, T. D., Lynds, C. R., Rieke, G. H. & Ekers, R. D. 1975, *ApJ*, 198, 261
- Urry, C. M. & Padovani, P. 1995, *PASP*, 107, 803
- Valtaoja, E., Lähteenmäki, A., Teräsraanta, H., & Lainela, M. 1999, *ApJS*, 120, 95
- Valtaoja, E., Teräsraanta, H., Urpo, S., et al. 1992, *A&A*, 254, 71
- Valtonen, M., Kidger, M., Lehto, H., & Poyner, G. 2008, *A&A*, 477, 407
- Venturi, T., Dallacasa, A., Orfei, A., et al. 2001, *A&A*, 379, 755
- Vermeulen, R. C., Ogle, P. M., Tran, H. D., et al. 1995, *ApJ*, 452, L5
- Véron-Cetty, M.-P. & Véron, P. 2000, *ESO Scientific Report no. 19*. 1
- Véron-Cetty, M. P. & Véron, P. 2006, *A&A*, 455, 773
- Villata, M. & Raiteri, C. M. 1999, *A&A*, 347, 30
- Wagner, S. J. & Witzel, A. 1995, *ARA&A*, 33, 163
- Weistrop, D., Hintzen, P., Romanishin, W. & Shaffer, D. B. 1984, *Bulletin of the American Astronomical Society*, 16, 521
- Wiklind, T. & Combes, F. 1997, *A&A*, 328, 48
- Wright, A. E., Ables, J. G., & Allen, D. A. 1983, *MNRAS*, 205, 793

TABLE 1

THE SOURCE SAMPLE OF 24 BLOs. COLUMN (8) INDICATES WHETHER THE SOURCE IS INCLUDED IN THE FLARE ANALYSIS. SEE TEXT FOR DETAILS.

Source	Alias	R.A.(J2000)	Dec(J2000)	z	D_{var}	Class	Flare analysis	ref. for z
0109+224	S2 0109+22	01 ^h 12 ^m 05.8 ^s	+22°44'39"	LBL	*	...
0235+164	AO 0235+164	02 ^h 38 ^m 38.8 ^s	+16°36'59"	0.940	24.0	LBL	*	3
0422+004	PKS 0422+004	04 ^h 24 ^m 46.8 ^s	+00°36'07"	0.310	...	IBL	*	9
0716+714	S5 0716+714	07 ^h 21 ^m 53.3 ^s	+71°20'6"	0.310	10.9	LBL	*	8
0735+178	PKS 0735+178	07 ^h 38 ^m 07.4 ^s	+17°42'19"	0.424	3.8	LBL	*	5
0754+100	PKS 0754+100	07 ^h 57 ^m 06.7 ^s	+09°56'35"	0.266	5.6	LBL	*	2
0814+425	OJ 425	08 ^h 18 ^m 16.1 ^s	+42°22'46"	0.245	4.6	LBL		1
0851+202	OJ 287	08 ^h 54 ^m 48.8 ^s	+20°06'30"	0.306	17.0	LBL	*	12
0954+658	S4 0954+65	09 ^h 58 ^m 47.2 ^s	+65°33'54"	0.367	6.2	LBL		7
1101+384	Mark 421	11 ^h 04 ^m 27.2 ^s	+38°12'32"	0.031	...	HBL		16
1147+245	B2 1147+24	11 ^h 50 ^m 19.2 ^s	+24°17'54"	0.200	...	LBL		10
1219+285	ON 231	12 ^h 21 ^m 31.7 ^s	+28°13'58"	0.102	1.2	IBL		18
1308+326	AUCVn	13 ^h 10 ^m 28.7 ^s	+32°30'43.8"	0.997	15.4	LBL	*	15
1413+135	PKS 1413+135	14 ^h 15 ^m 58.8 ^s	+13°20'24"	0.247	12.2	LBL	*	19
1418+546	OQ 530	14 ^h 19 ^m 46.6 ^s	+54°23'14"	0.151	5.1	LBL		13
1538+149	4C 14.60	15 ^h 40 ^m 46.5 ^s	+14°47'45.9"	0.605	4.3	IBL		14
1652+398	Mark 501	16 ^h 53 ^m 52.2 ^s	+39°45'36"	0.034	...	HBL		16
1749+096	OT 081	17 ^h 51 ^m 32.7 ^s	+09°39'01"	0.322	12.0	LBL	*	11
1803+784	S5 1803+784	18 ^h 00 ^m 45.4 ^s	+78°28'04"	0.684	12.2	LBL		6
1807+698	3C 371.0	18 ^h 06 ^m 50.7 ^s	+69°49'28"	0.051	1.1	IBL		4
1823+568	4C 56.27	18 ^h 24 ^m 07.1 ^s	+56°51'01.5"	0.663	6.4	LBL		7
2007+776	S5 2007+77	20 ^h 05 ^m 31.1 ^s	+77°52'43"	0.342	7.9	LBL	*	13
2200+420	BL Lac	22 ^h 02 ^m 43.3 ^s	+42°16'39"	0.069	7.3	LBL	*	17
2223-052	3C 446	22 ^h 25 ^m 45.1 ^s	-04°56'34"	1.404	16.0	LBL	*	20

References. — (1) Britzen et al. (2008); (2) Carangelo et al. (2003); (3) Cohen et al. (1987); (4) De Grijp et al. (1992); (5) Hewitt & Burbidge (1987); (6) Hewitt & Burbidge (1989); (7) Lawrence et al. (1986); (8) Nilsson et al. (2008); (9) Smith & Nair (1995); (10) Sowards-Emmerd et al. (2005); (11) Stickel et al. (1988); (12) Stickel et al. (1989); (13) Stickel et al. (1991); (14) Stickel et al. (1993); (15) Tytler & Fan (1992); (16) Ulrich et al. (1975); (17) Vermeulen et al. (1995); (18) Weistrop et al. (1984); (19) Wiklind & Combes (1997); (20) Wright et al. (1983)

TABLE 2

THE MOST SIGNIFICANT TIMESCALES OBTAINED FOR THE SAMPLE SOURCES USING THE STRUCTURE FUNCTION (T_{SF}), THE DISCRETE CORRELATION FUNCTION (T_{DCF}) AND THE LOMB-SCARGLE PERIODOGRAM (T_P). ALL TIME SCALES ARE IN THE OBSERVER'S FRAME.

Source	Alias	ν [GHz]	T_{SF} [yr]	T_{DCF} [yr]	T_P [yr]	Note
0109+224	S2 0109+22	4.8	1.358	1.848	...	1
0109+224	S2 0109+22	8	4.817	7.324	...	1
0109+224	S2 0109+22	14.5	1.078	5.818	...	1, 2
0109+224	S2 0109+22	22	0.857	7.734
0109+224	S2 0109+22	37	1.918	2.943
0235+164	AO 0235+164	4.8	0.961	1.848	11.523	...
0235+164	AO 0235+164	8	0.606	1.848	5.615	2
0235+164	AO 0235+164	14.5	0.857	5.544	5.658	...
0235+164	AO 0235+164	22	0.961	5.681	5.609	...
0235+164	AO 0235+164	37	2.709	3.901
0235+164	AO 0235+164	90	0.763	1.848
0422+004	PKS 0422+004	4.8	≥ 10.784	7.050	...	1, 2
0422+004	PKS 0422+004	8	≥ 10.784	7.871	...	1
0422+004	PKS 0422+004	14.5	3.826	6.092	...	1
0422+004	PKS 0422+004	22	≥ 9.612
0422+004	PKS 0422+004	37	2.709
0716+714	S5 0716+714	4.8	0.961	5.818	5.584	...
0716+714	S5 0716+714	8	≥ 8.566	5.270	4.213	...
0716+714	S5 0716+714	14.5	0.192	1.985
0716+714	S5 0716+714	22	≥ 12.100	1.711	...	2
0716+714	S5 0716+714	37	0.680	2.259	2.232	2
0716+714	S5 0716+714	90	≥ 6.805
0735+178	PKS 0735+178	4.8	3.826
0735+178	PKS 0735+178	8	5.405	...	14.105	...
0735+178	PKS 0735+178	14.5	3.826
0735+178	PKS 0735+178	22	6.065
0735+178	PKS 0735+178	37	2.152
0735+178	PKS 0735+178	90	2.709
0754+100	PKS 0754+100	4.8	2.414	7.050	10.037	...
0754+100	PKS 0754+100	8	3.039	7.871	10.814	2
0754+100	PKS 0754+100	14.5	4.293	10.883	10.628	...
0754+100	PKS 0754+100	22	0.541	3.354	6.255	...
0754+100	PKS 0754+100	37	1.210	2.806	2.819	2
0814+425	OJ 425	4.8	≥ 10.784
0814+425	OJ 425	8	0.606	...	14.070	...
0814+425	OJ 425	14.5	7.635
0814+425	OJ 425	22	≥ 5.405
0814+425	OJ 425	37	≥ 4.293
0851+202	OJ 287	4.8	0.341
0851+202	OJ 287	8	0.215	6.502	...	2
0851+202	OJ 287	14.5	0.241
0851+202	OJ 287	22	0.304
0851+202	OJ 287	37	0.482	5.818
0851+202	OJ 287	90	0.241	5.133	1.031	2
0851+202	OJ 287	230	...	4.038	...	2
0954+658	S4 0954+65	4.8	10.784
0954+658	S4 0954+65	8	3.039	5.955	...	1
0954+658	S4 0954+65	14.5	12.100	3.217	...	1
0954+658	S4 0954+65	22	1.210	2.806	...	1
0954+658	S4 0954+65	37	0.383	2.533	...	1
1101+384	Mark 421	4.8	0.215	1.164	...	1
1101+384	Mark 421	8	0.271	1.848	5.236	1
1101+384	Mark 421	14.5	0.241	2.806	9.604	1, 2

TABLE 2—*Continued*

Source	Alias	ν [GHz]	T_{SF} [yr]	T_{DCF} [yr]	T_P [yr]	Note
1101+384	Mark 421	22	0.271	0.890	0.800	1, 2
1101+384	Mark 421	37	...	1.848	...	1, 2
1147+245	B2 1147+24	8	...	4.860	...	1
1147+245	B2 1147+24	22	...	3.354	...	1
1147+245	B2 1147+24	37
1219+285	ON 231	4.8	6.805	10.609
1219+285	ON 231	8	≥ 24.143
1219+285	ON 231	14.5	≥ 24.143
1219+285	ON 231	22	≥ 21.518	7.324	7.962	...
1219+285	ON 231	37	4.293	7.324	8.768	...
1308+326	AUCVn	4.8	3.410	11.704
1308+326	AUCVn	8	4.293	10.746	14.594	...
1308+326	AUCVn	14.5	3.039	10.335	8.890	...
1308+326	AUCVn	22	2.709
1308+326	AUCVn	37	3.039	10.472	12.002	...
1308+326	AUCVn	90	...	3.765	...	3
1413+135	PKS 1413+135	4.8	2.152	9.377	7.618	1
1413+135	PKS 1413+135	8	2.709	9.377	8.206	...
1413+135	PKS 1413+135	14.5	2.709	6.776	9.109	...
1413+135	PKS 1413+135	22	1.709	3.901	7.682	...
1413+135	PKS 1413+135	37	1.523	3.901	8.067	...
1413+135	PKS 1413+135	90	...	2.259
1418+546	OQ 530	4.8	1.210	3.901
1418+546	OQ 530	8	1.078	2.533	...	2
1418+546	OQ 530	14.5	1.523	4.723	...	2
1418+546	OQ 530	22	≥ 7.635	4.175
1418+546	OQ 530	37	0.606	7.050
1538+149	4C 14.60	4.8	5.405	5.133	...	1
1538+149	4C 14.60	8	2.152
1538+149	4C 14.60	14.5	1.358
1538+149	4C 14.60	22	7.635
1538+149	4C 14.60	37	7.635	6.913	...	1
1652+398	Mark 501	4.8	2.709	4.038	...	1
1652+398	Mark 501	8	4.817
1652+398	Mark 501	14.5	3.039	10.746	...	1
1652+398	Mark 501	22	≥ 12.100	1.300	4.958	1
1652+398	Mark 501	37	≥ 12.100	3.354	8.454	1
1749+096	PKS 1749+096	4.8	1.358	4.449
1749+096	PKS 1749+096	8	2.152	6.776	6.956	...
1749+096	PKS 1749+096	14.5	1.078	2.533	3.043	...
1749+096	PKS 1749+096	22	0.606	2.806	3.055	...
1749+096	PKS 1749+096	37	0.341	2.122	9.813	2
1749+096	PKS 1749+096	90	3.040	1.300	1.944	2
1803+784	S5 1803+784	4.8	0.857	10.883	10.849	...
1803+784	S5 1803+784	8	1.918	2.943	...	2
1803+784	S5 1803+784	14.5	2.152	4.312	9.785	...
1803+784	S5 1803+784	22	...	4.723
1803+784	S5 1803+784	37	...	2.806
1807+698	3C 371.0	4.8	3.826
1807+698	3C 371.0	8	10.784	9.240	...	2
1807+698	3C 371.0	14.5	4.817
1807+698	3C 371.0	22	...	1.300
1807+698	3C 371.0	37	...	2.533	...	1

TABLE 2—*Continued*

Source	Alias	ν [GHz]	T_{SF} [yr]	T_{DCF} [yr]	T_P [yr]	Note
1823+568	4C 56.27	4.8	3.039	9.377
1823+568	4C 56.27	8	3.039	7.871
1823+568	4C 56.27	14.5	1.918	2.806
1823+568	4C 56.27	22	4.293
1823+568	4C 56.27	37	2.709
2007+776	S5 2007+77	4.8	1.523	3.354
2007+776	S5 2007+77	8	0.680	2.259
2007+776	S5 2007+77	14.5	1.709
2007+776	S5 2007+77	22	3.826
2007+776	S5 2007+77	37	...	3.080	3.061	...
2200+420	BL Lac	4.8	3.826	7.461	8.514	...
2200+420	BL Lac	8	0.763	2.806	3.803	...
2200+420	BL Lac	14.5	0.961	7.461	8.267	...
2200+420	BL Lac	22	2.414	7.734	8.730	2
2200+420	BL Lac	37	0.482	3.491	8.481	2
2200+420	BL Lac	90	...	4.449	5.984	...
2223-052	3C 446	4.8	3.410	9.103	11.934	...
2223-052	3C 446	8	1.523	8.419	15.241	...
2223-052	3C 446	14.5	2.709	11.157	5.710	...
2223-052	3C 446	22	2.709
2223-052	3C 446	37	3.039
2223-052	3C 446	90	1.358	5.955

NOTE.—1 = faint source, 2 = multiple time scales, 3 = exceptionally large errors in T_{DCF} . See text for details.

TABLE 3

THE NUMBER OF FLARES INCLUDED IN THE ANALYSIS AND THE MEAN VALUES OF THE DURATION, RISE TIME, DECAY TIME, ABSOLUTE PEAK FLUX AND RELATIVE PEAK FLUX FOR THE 13 FLARING SOURCES IN OUR SAMPLE. THE PARAMETERS HAVE BEEN CALCULATED FOR ALL FREQUENCY BANDS AND SEPARATELY FOR 37 GHz.

Source	Frequency	Number of flares	Duration [yr]	Rise time [yr]	Decay time [yr]	Absolute peak flux [Jy]	Relative peak flux [Jy]
S2 0109+22	All	3	3.9	1.3	2.6	1.6	1.1
	37 GHz	3	3.7	1.0	2.7	2.3	1.7
AO 0235+164	All	4	2.3	1.2	1.1	4.5	3.6
	37 GHz	4	2.4	1.4	1.1	5.3	4.2
PKS 0422+004	All	2	3.3	1.5	1.7	1.5	1.1
	37 GHz	2	2.0	0.6	1.3	1.9	1.3
S5 0716+714	All	2	3.0	1.2	1.8	2.9	2.4
	37 GHz	2	3.1	0.9	2.2	4.4	4.1
PKS 0735+178	All	1	10.8	2.9	7.8	4.6	3.5
	37 GHz	1	10.7	1.9	8.8	5.3	4.4
PKS 0754+100	All	2	3.4	1.5	2.0	2.3	1.3
	37 GHz	2	3.3	1.0	2.2	2.7	1.7
OJ 287	All	9	1.4	0.7	0.7	4.9	2.7
	37 GHz	9	1.3	0.7	0.6	5.9	3.5
1308+326	All	2	12.8	5.9	6.9	4.1	3.5
	37 GHz	2	13.2	3.9	8.1	3.5	2.9
PKS 1413+135	All	2	4.8	2.2	2.5	3.0	2.2
	37 GHz	2	4.8	2.6	2.2	3.5	3.0
PKS 1749+096	All	5	1.7	0.9	0.8	6.4	4.3
	37 GHz	5	1.7	0.8	0.9	7.5	5.2
S5 2007+77	All	1	3.3	1.5	1.8	3.3	2.1
	37 GHz	1	3.3	1.5	1.9	3.0	2.2
BL Lac	All	9	1.8	0.9	0.9	5.0	2.9
	37 GHz	9	1.6	0.8	0.8	5.1	3.2
3C 446	All	3	5.8	2.7	3.1	7.8	4.6
	37 GHz	3	5.4	3.1	2.3	8.1	5.4

Table 4: Minimum, maximum, mean and median values of flare duration and absolute and relative peak fluxes (both $S_{\max} - S_{\min}$ and S_{\max}/S_{\min}) for all frequencies used in the analysis. Values are also shown for duration and absolute flux of the flares normalized to the values at 22 GHz.

ν [GHz]	Duration [yr]				Normalized duration			
	min.	max.	mean	median	min.	max.	mean	median
4.8	0.6	12.7	3.5	2.7	0.4	2.2	1.1	1.0
8	0.7	12.8	3.4	2.7	0.4	3.2	1.1	1.1
14.5	0.3	12.4	3.0	2.4	0.7	3.0	1.1	1.0
22	0.3	13.0	2.9	2.3	1.0	1.0	1.0	1.0
37	0.4	13.2	2.9	2.4	0.7	1.9	1.0	1.0
90	0.6	10.3	3.1	2.3	0.7	1.7	1.0	1.0
230	0.9	9.9	3.4	2.3	0.6	1.1	0.9	0.9
ν [GHz]	Absolute peak flux [Jy]				Normalized abs. peak flux			
	min.	max.	mean	median	min.	max.	mean	median
4.8	0.7	7.1	3.4	3.2	0.28	1.08	0.67	0.63
8	0.9	8.0	4.0	4.3	0.45	1.08	0.80	0.81
14.5	0.8	9.0	4.5	4.2	0.53	1.12	0.90	0.91
22	1.2	10.7	5.0	4.9	1.0	1.0	1.0	1.0
37	1.4	10.9	5.1	5.1	0.81	1.28	1.03	1.04
90	1.3	12.1	5.1	4.4	0.56	1.89	0.98	0.90
230	1.2	11.7	4.4	3.2	0.42	1.09	0.70	0.67
ν [GHz]	Relative peak flux [Jy]				Relative peak flux (S_{\max}/S_{\min})			
	min.	max.	mean	median	min.	max.	mean	median
4.8	0.4	4.8	1.9	1.7	1.4	17.8	3.1	2.2
8	0.7	5.1	2.4	2.1	1.4	16.7	3.7	2.6
14.5	0.8	5.8	2.8	2.4	1.5	18.4	3.9	2.6
22	0.8	7.1	3.2	2.8	1.8	11.1	3.6	2.8
37	1.0	7.6	3.5	3.1	1.8	18.5	4.4	3.3
90	0.6	9.4	3.5	2.8	1.6	12.2	4.0	2.9
230	0.9	10.1	3.3	1.9	1.8	7.1	4.2	3.7

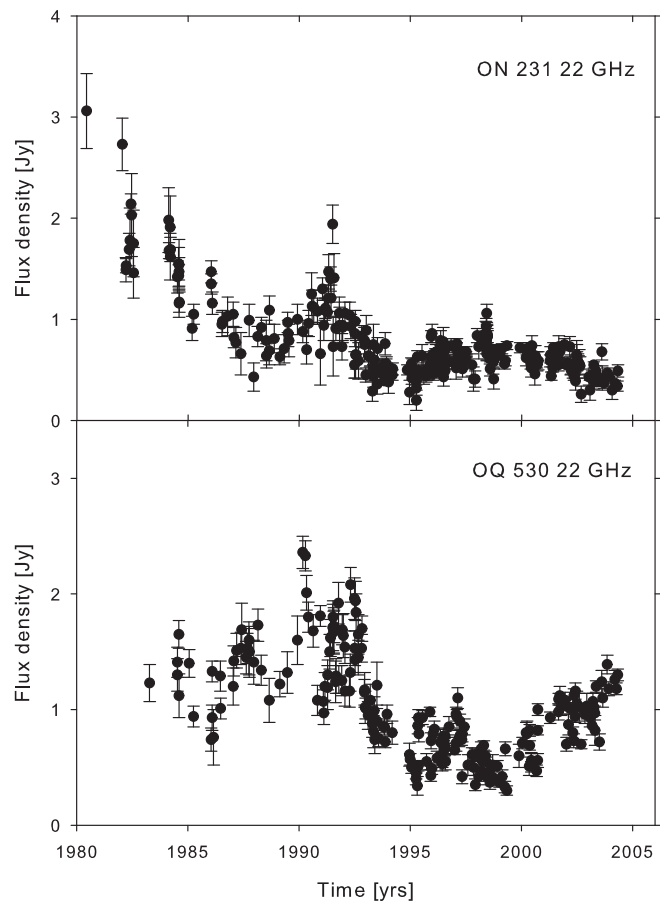


Fig. 1.— Flux curves of ON 231 (top panel) and OQ 530 (bottom panel) at 22 GHz

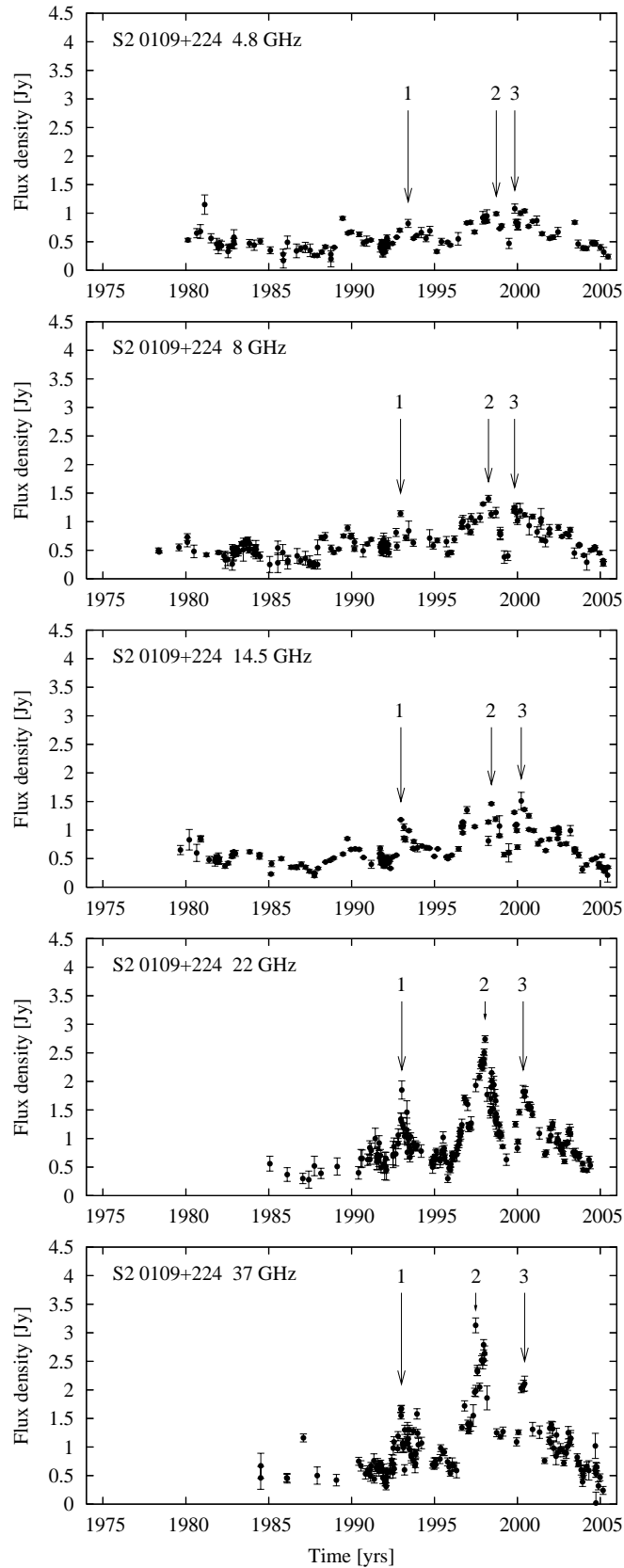


Fig. 2.— Flux curves of objects in the flare analysis. The peak of each flare included in the analysis is marked in the curve. Plots for all sources are available in the electronic edition of the journal.

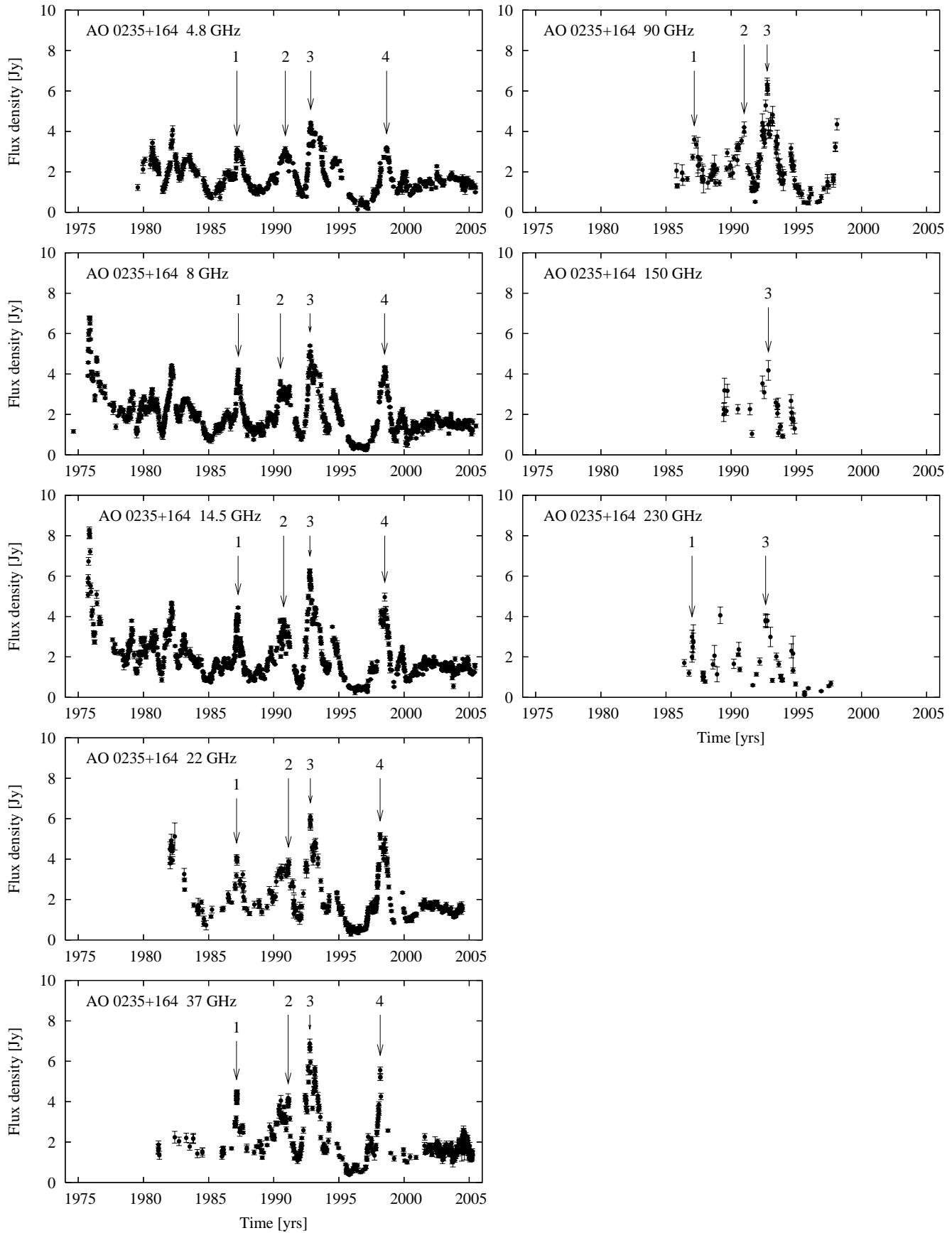


Fig. 2.2.— Flux curves of objects in the flare analysis. The peak of each flare included in the analysis is marked in the curve.

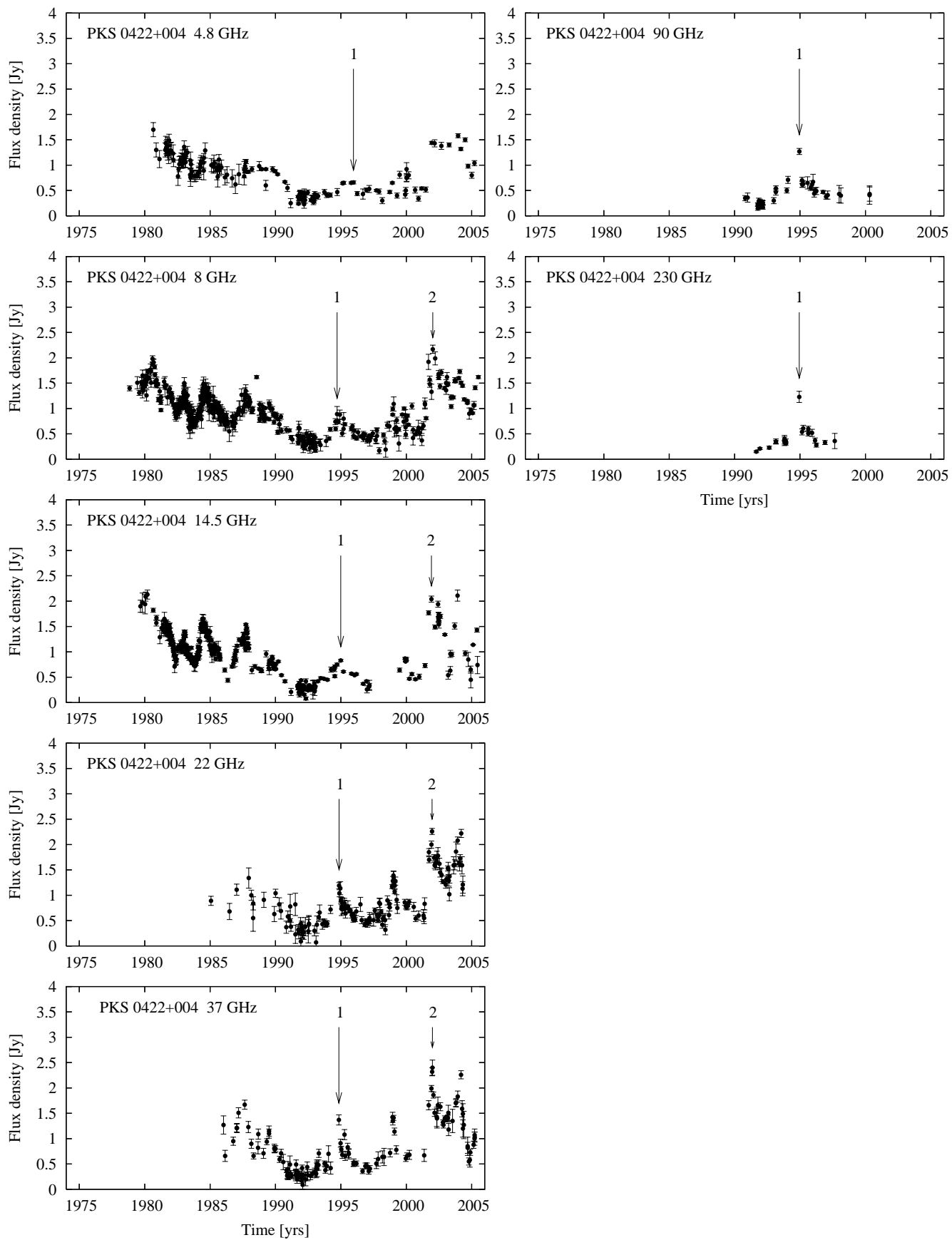


Fig. 2.3.— Flux curves of objects in the flare analysis. The peak of each flare included in the analysis is marked in the curve.

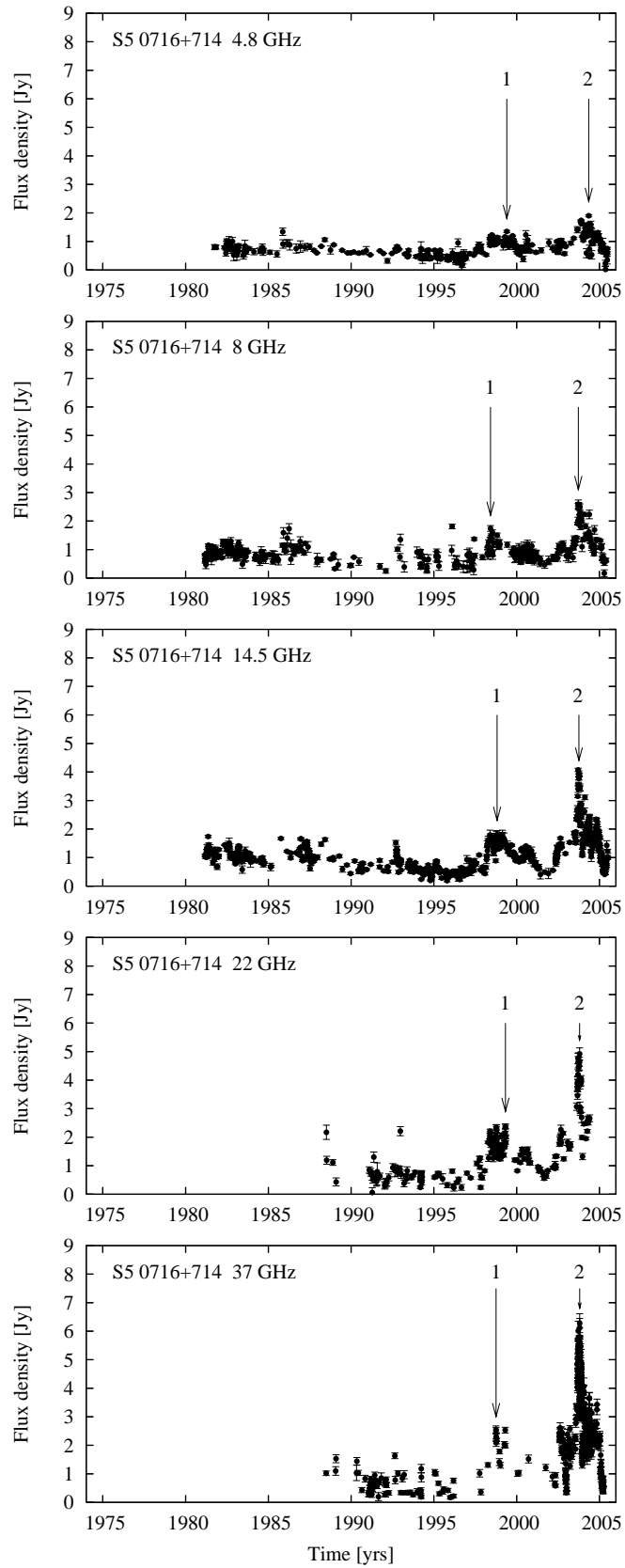


Fig. 2.4.— Flux curves of objects in the flare analysis. The peak of each flare included in the analysis is marked in the curve.

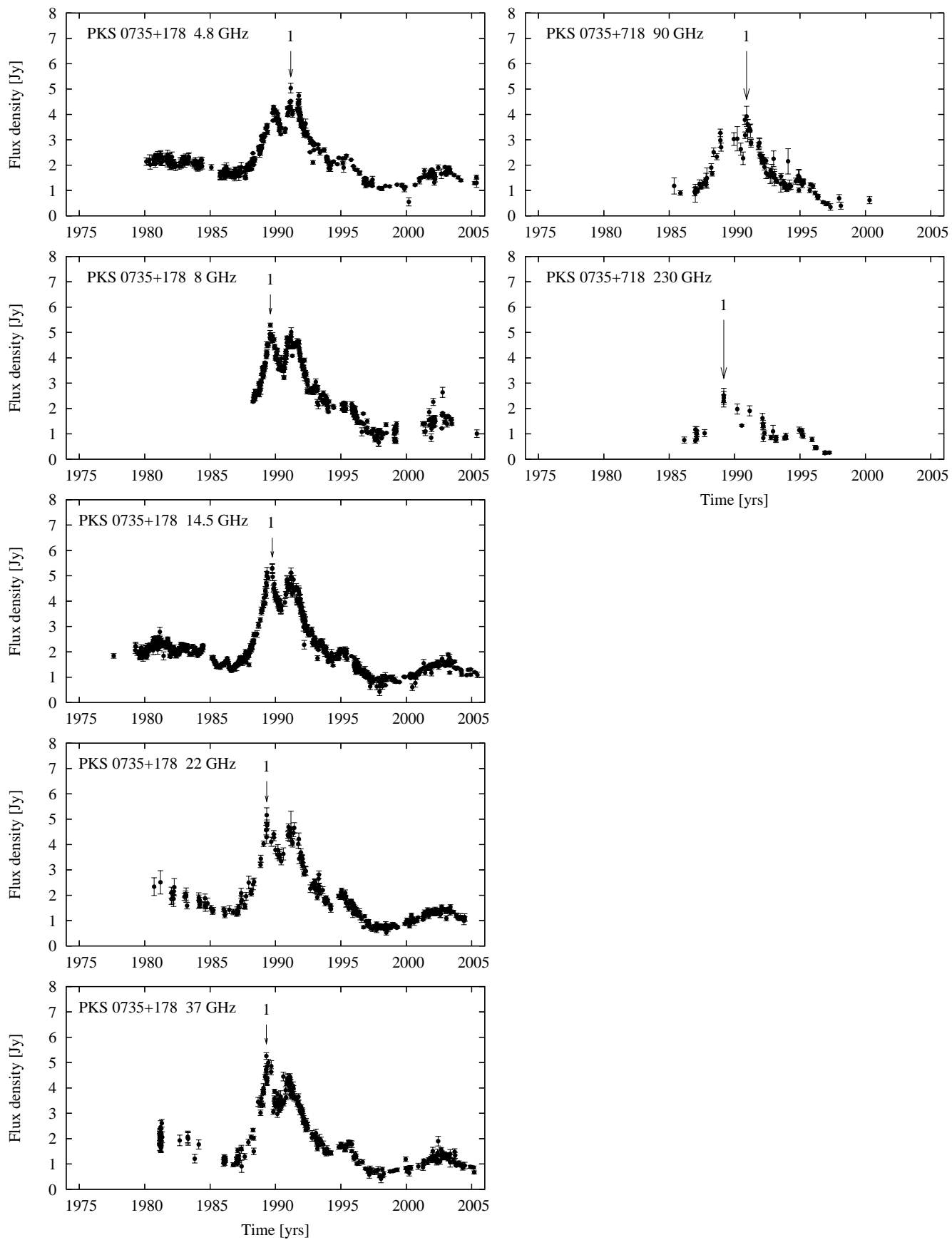


Fig. 2.5.— Flux curves of objects in the flare analysis. The peak of each flare included in the analysis is marked in the curve.

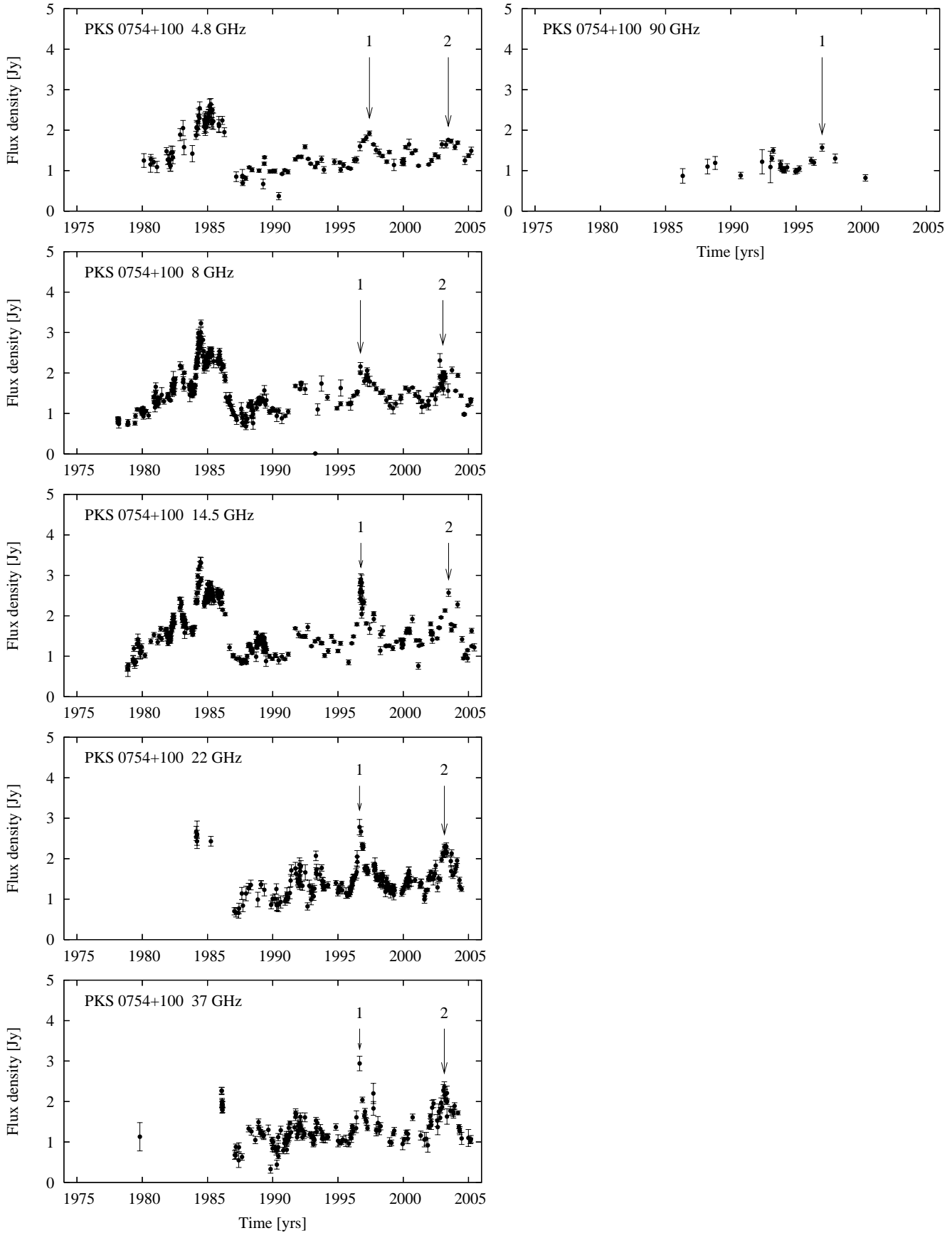


Fig. 2.6.— Flux curves of objects in the flare analysis. The peak of each flare included in the analysis is marked in the curve.

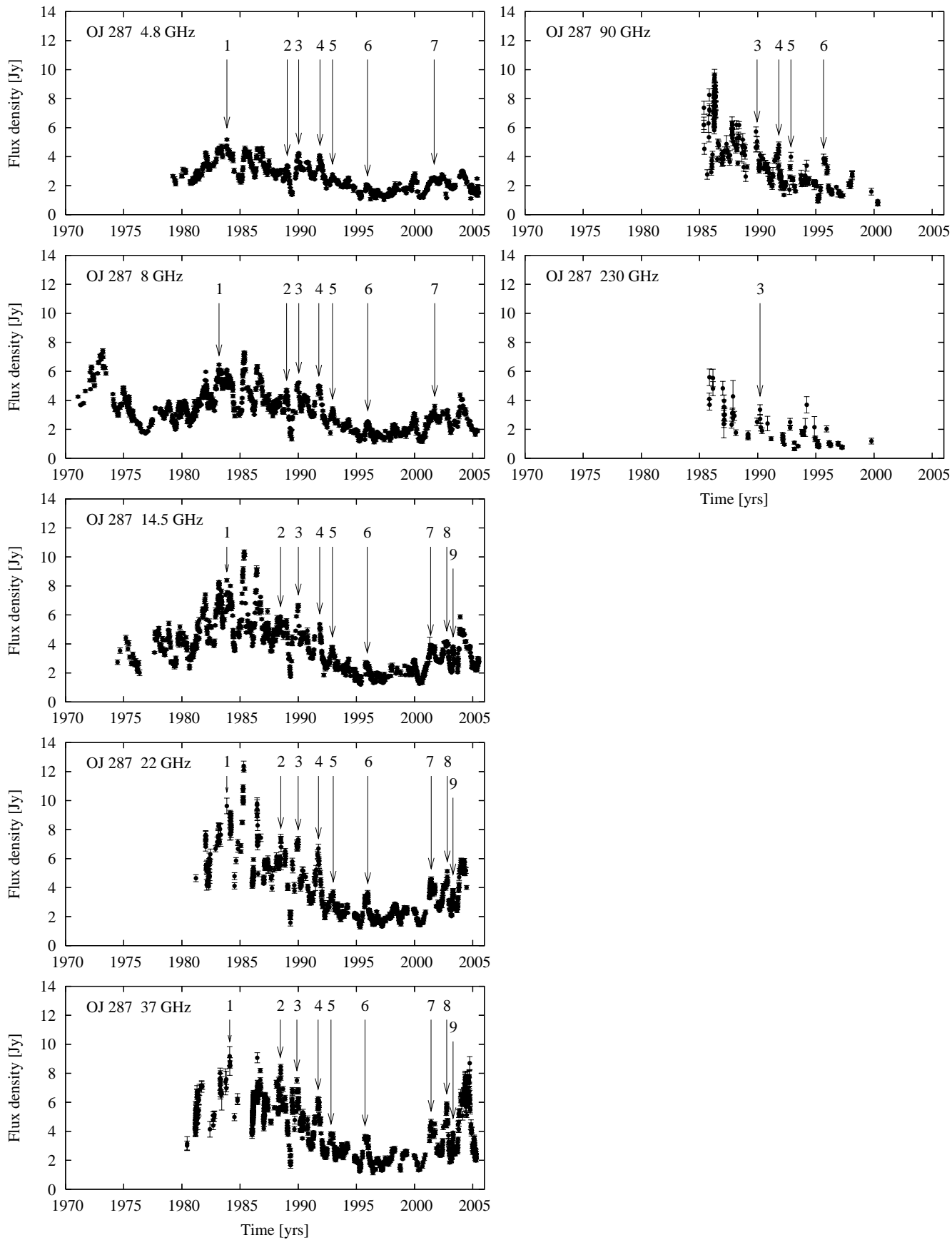


Fig. 2.7.— Flux curves of objects in the flare analysis. The peak of each flare included in the analysis is marked in the curve.

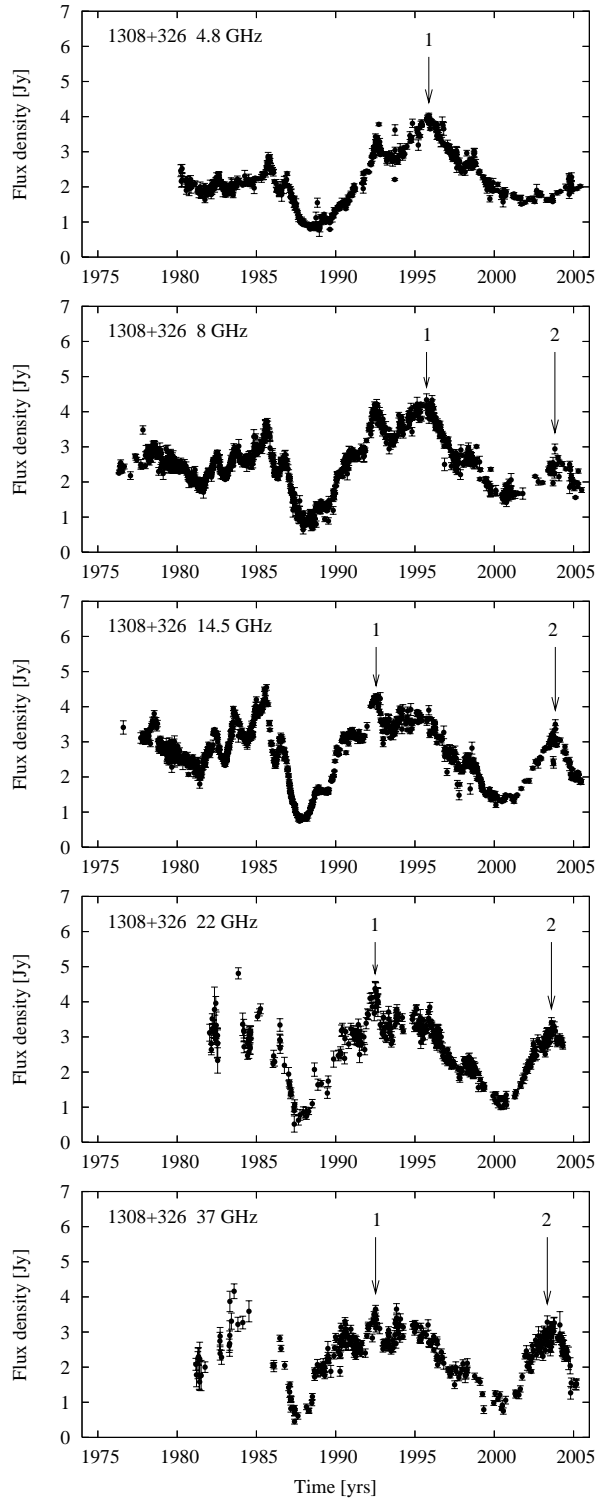


Fig. 2.8.— Flux curves of objects in the flare analysis. The peak of each flare included in the analysis is marked in the curve.

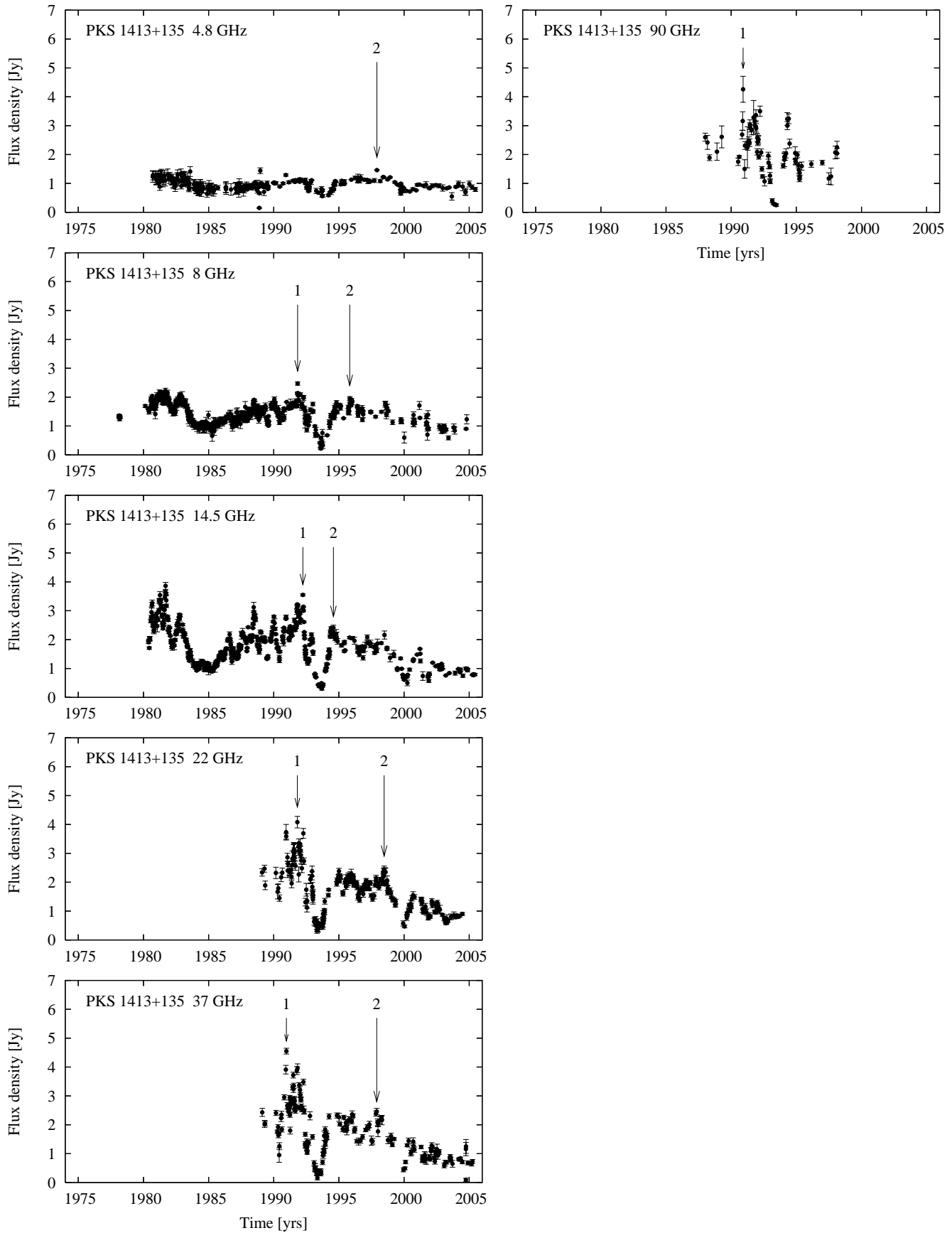


Fig. 2.9.— Flux curves of objects in the flare analysis. The peak of each flare included in the analysis is marked in the curve.

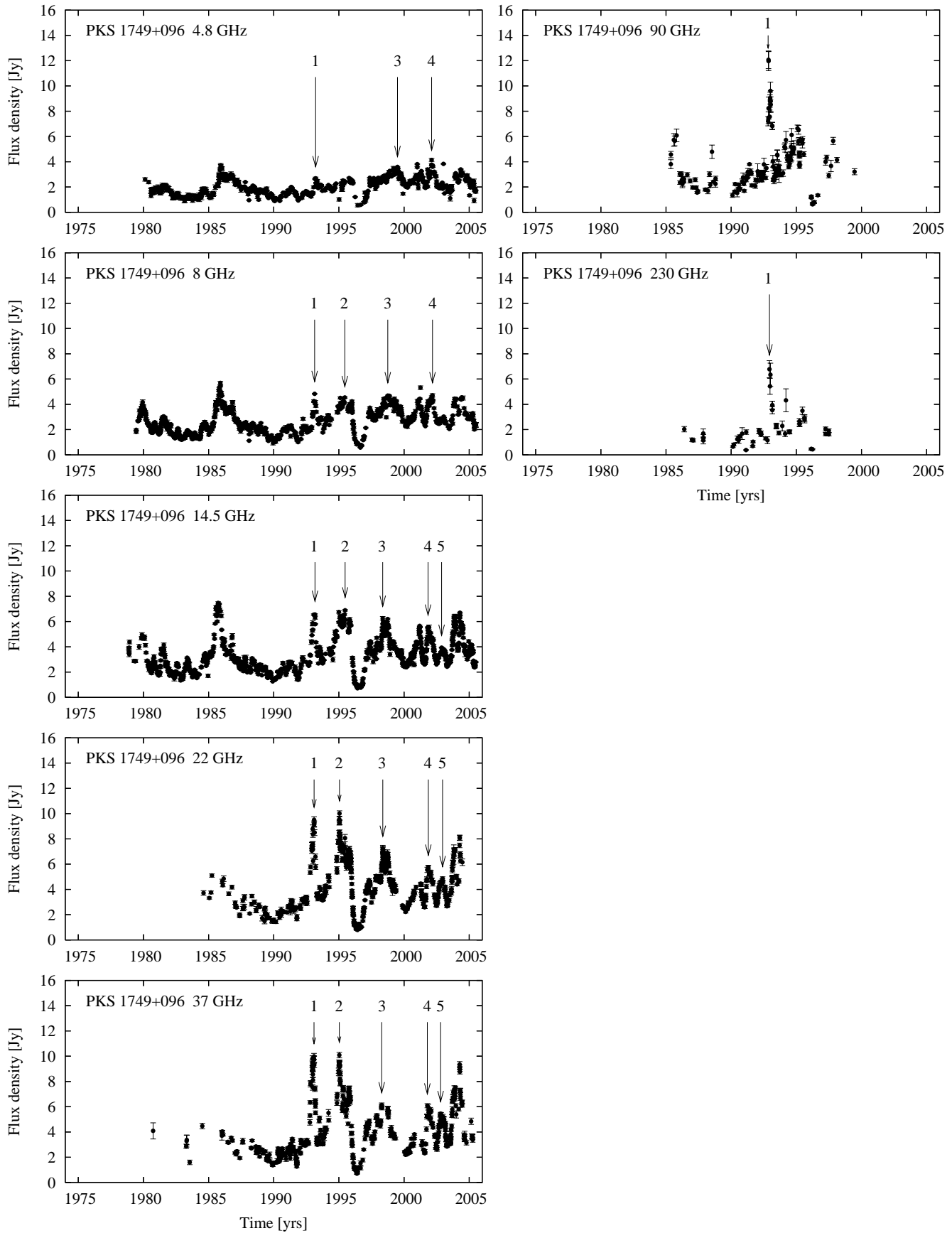


Fig. 2.10.— Flux curves of objects in the flare analysis. The peak of each flare included in the analysis is marked in the curve.

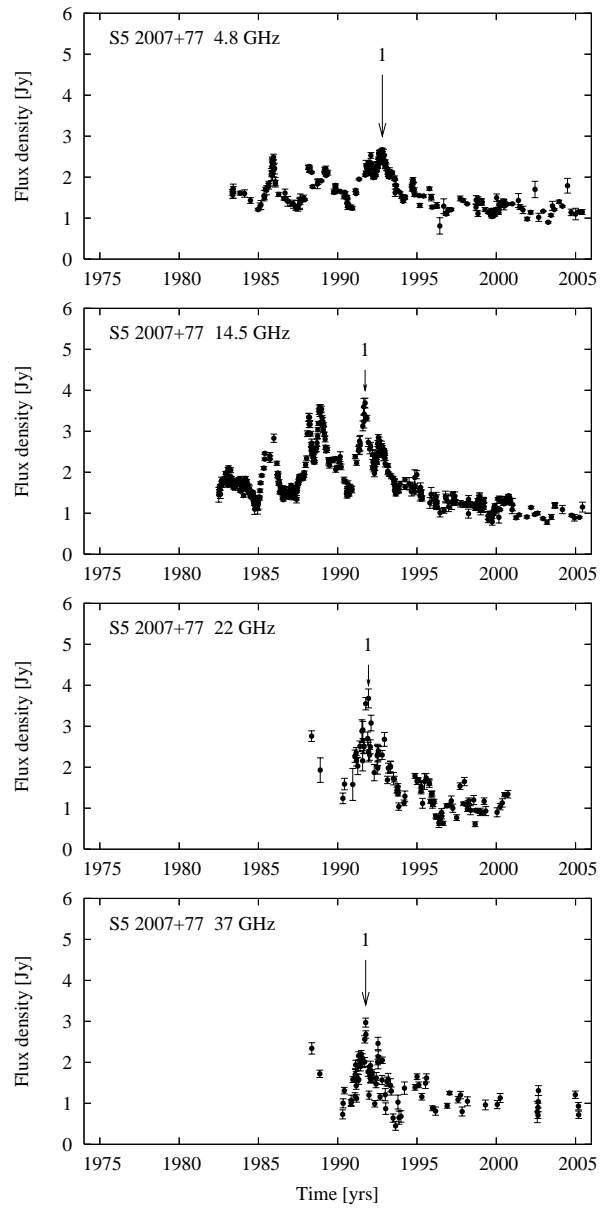


Fig. 2.11.— Flux curves of objects in the flare analysis. The peak of each flare included in the analysis is marked in the curve.

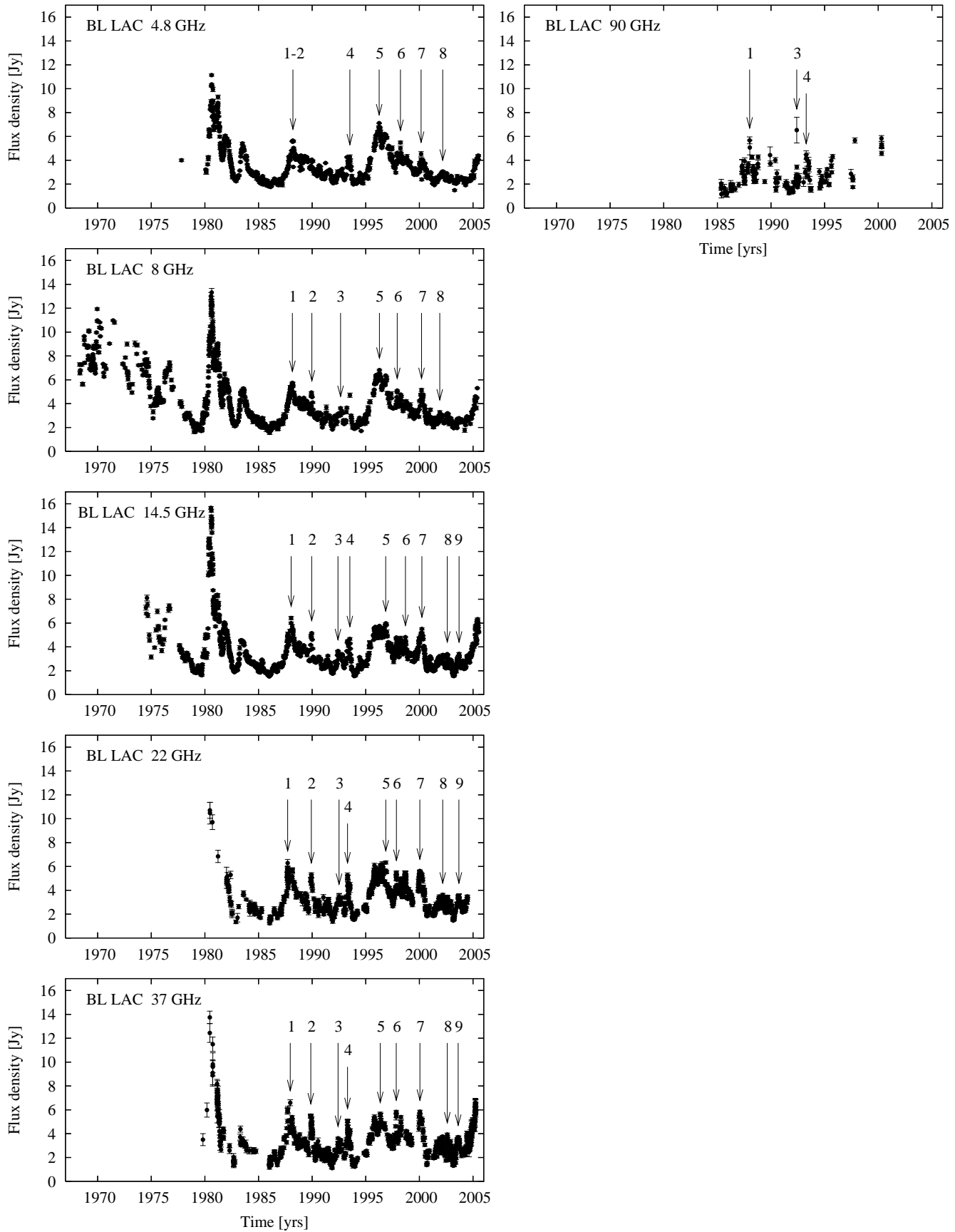


Fig. 2.12.— Flux curves of objects in the flare analysis. The peak of each flare included in the analysis is marked in the curve.

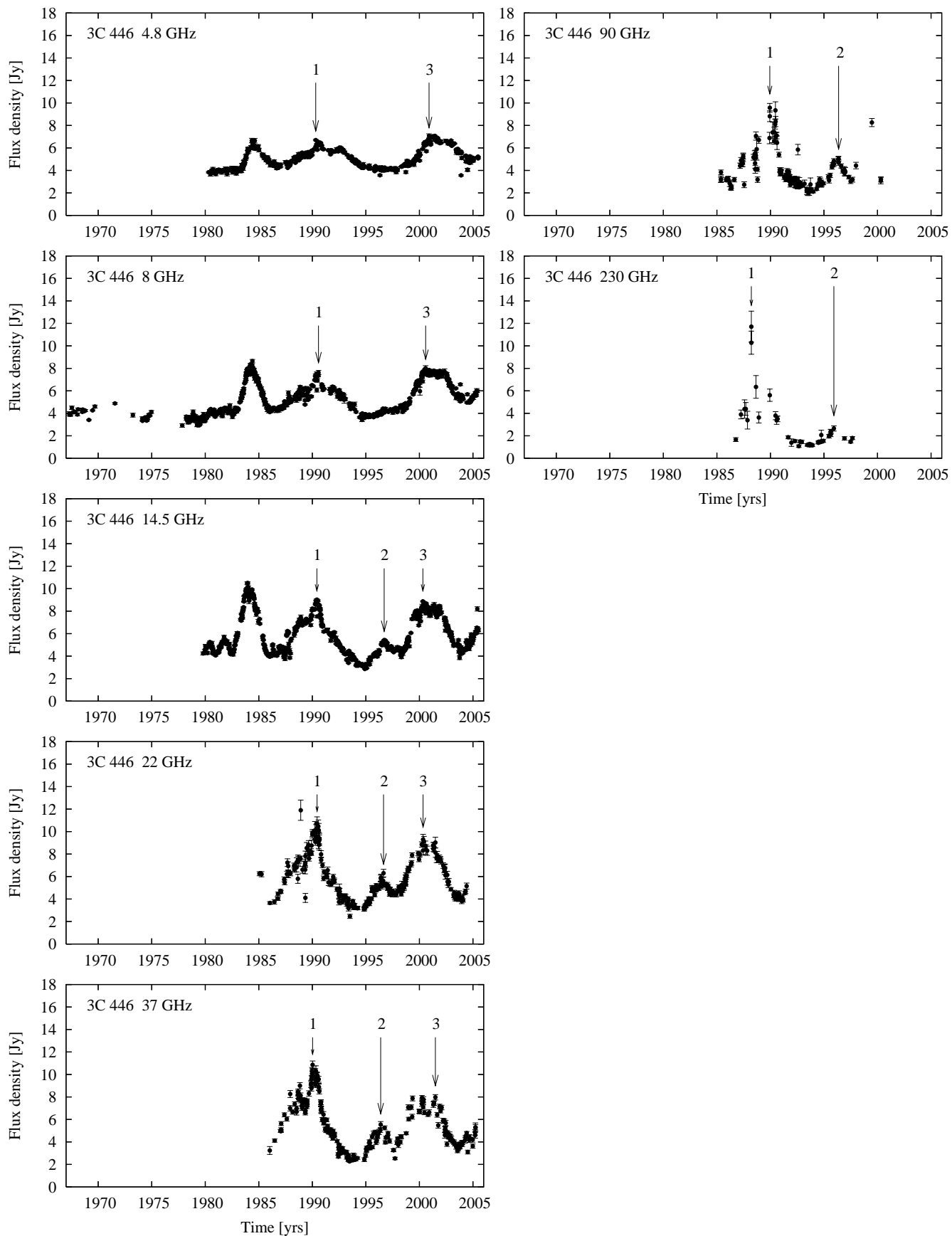


Fig. 2.13.— Flux curves of objects in the flare analysis. The peak of each flare included in the analysis is marked in the curve.

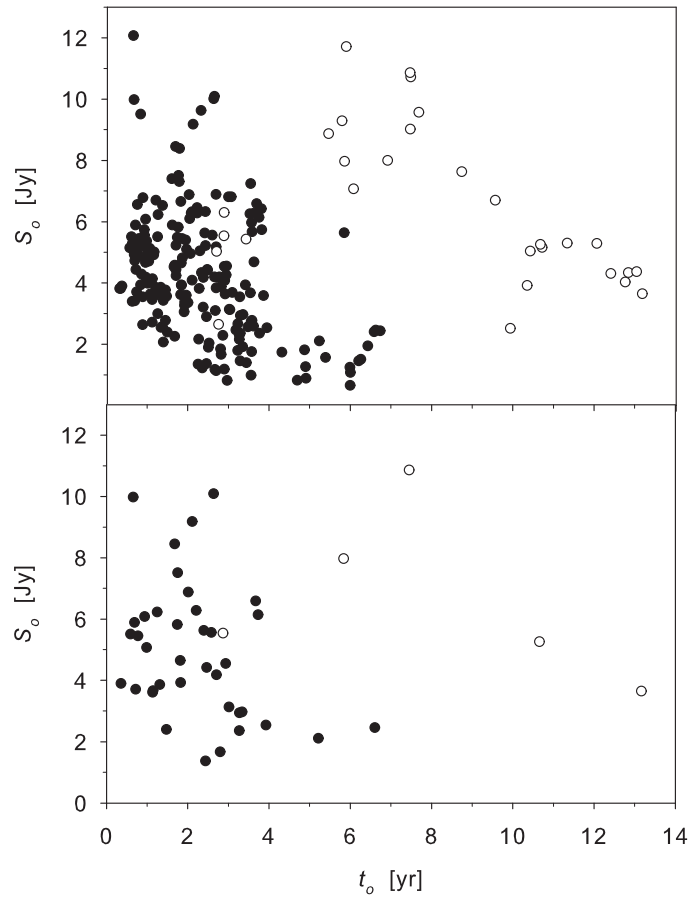


Fig. 3.— The absolute peak flux plotted against the duration of the flare, with all flares included (top panel) and only 37 GHz flares included (bottom panel). Datapoints of typical BLOs are marked with black circles, those of the three quasar-like objects are marked with open circles.

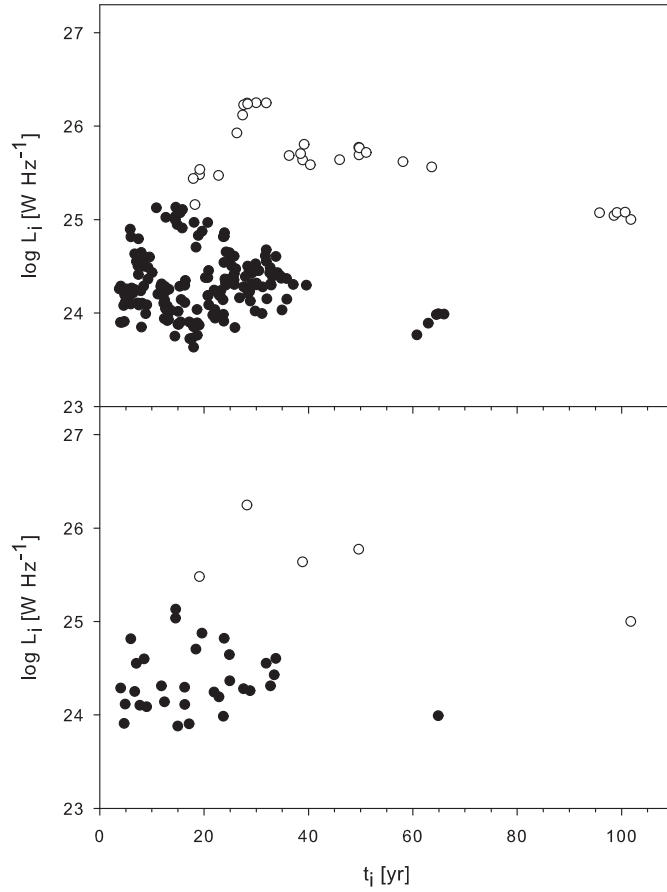


Fig. 4.— The Doppler-corrected flare peak luminosity plotted against the Doppler-corrected duration of the flare, with all flares included (top panel) and only 37 GHz flares included (bottom panel). Datapoints of typical BLOs are marked with black circles, those of the three quasar-like objects are marked with open circles.

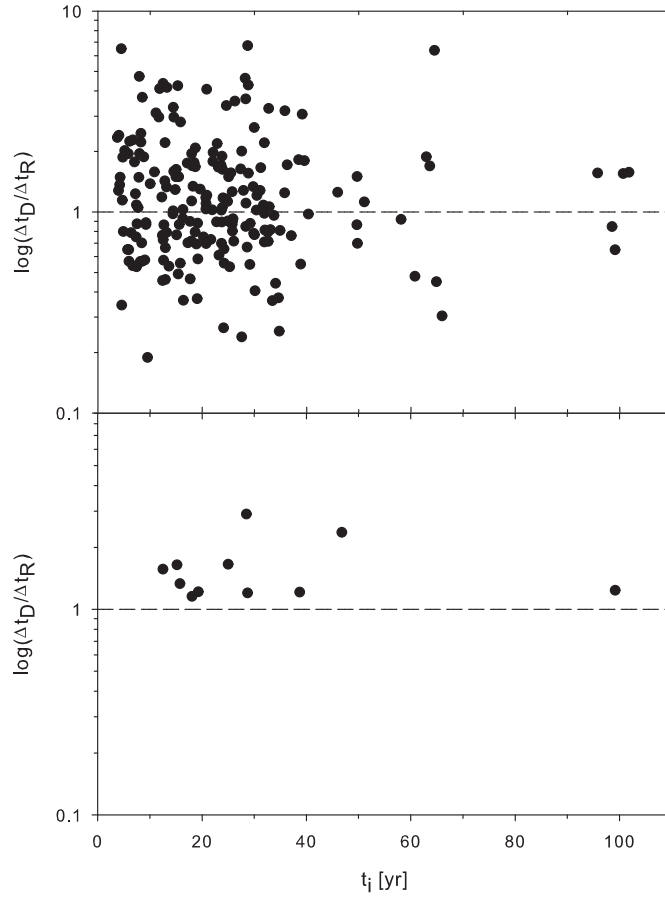


Fig. 5.— The ratio of the decay (Δt_D) and rise (Δt_R) times of all flares plotted against the duration of the flares. All values are Doppler-corrected. In the top panel all flares are included and in the bottom panel the source-specific mean values are plotted. For clarity, also the line $\Delta t_D / \Delta t_R = 1$, where the rise and decay times are of equal length, is included.

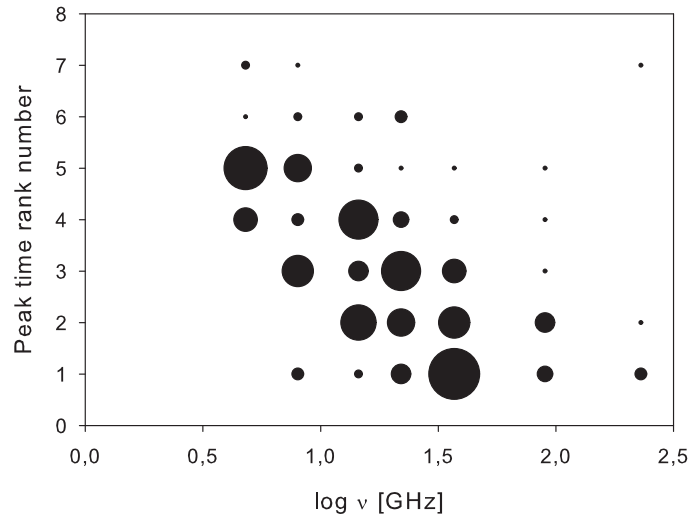


Fig. 6.— Peak time rank number plotted against frequency ν . The frequency band peaking first has been ranked 1.

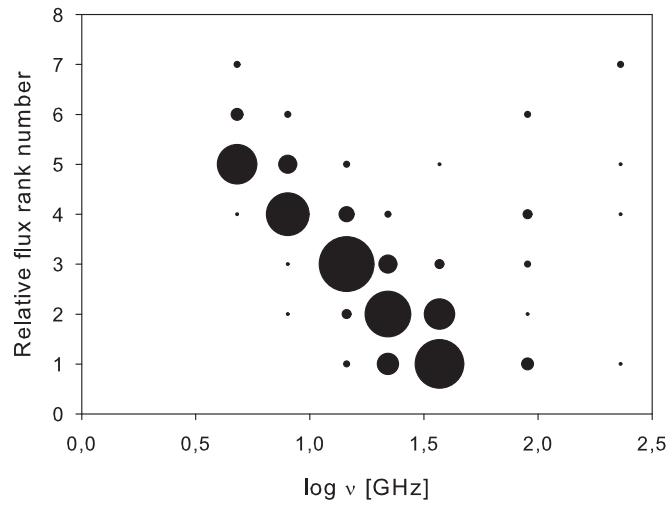


Fig. 7.— Relative peak flux rank number plotted against frequency. The frequency band having the highest relative peak flux has been ranked 1.

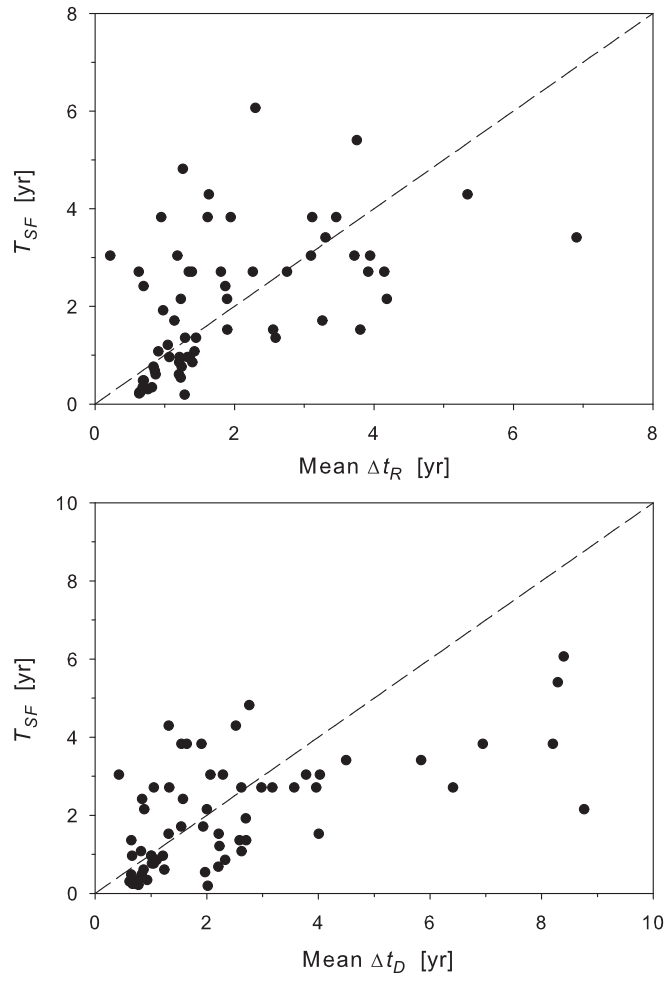


Fig. 8.— T_{SF} plotted against the rise times, Δt_R (top panel), and decay times, Δt_D (bottom panel), of the flares, averaged for each source and frequency. The dashed line represents a one-to-one correspondence.

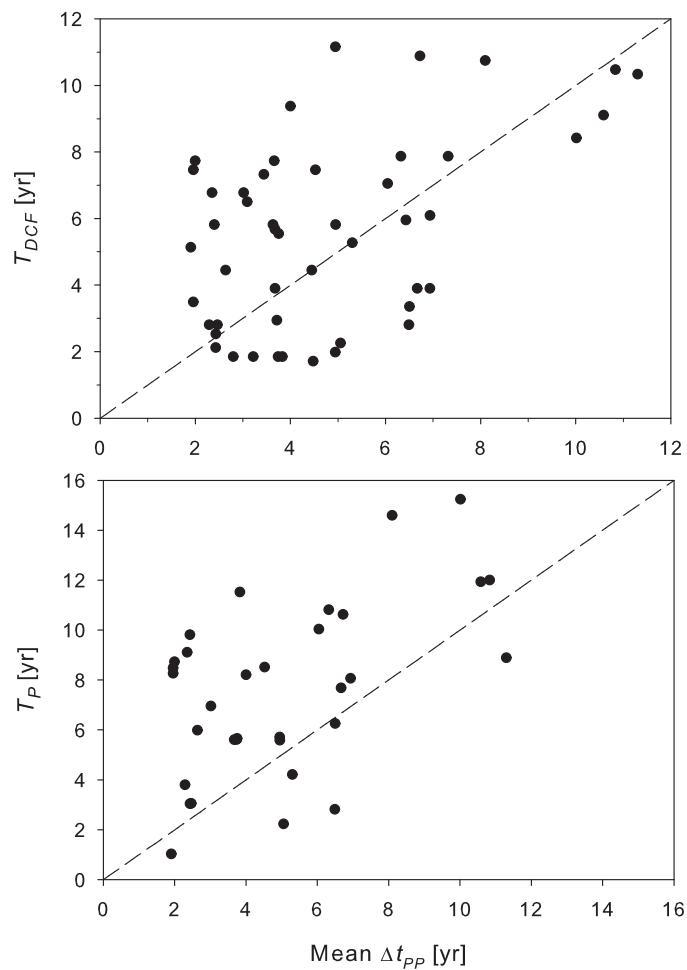


Fig. 9.— T_{DCF} and T_P plotted against the peak-to-peak intervals, Δt_{PP} (top panel) of the flares, averaged for each source and frequency. The dashed line represents a one-to-one correspondence.